MOUNTAIN-PLAINS CONSORTIUM

MPC 15-286 | F. Yazdani

Damage Assessment, Characterization, and Modeling for Enhanced Design of Concrete Bridge Decks in Cold Regions

MPC
MOUNTAIN-PLAINS CONSORTIUM

A University Transportation Center sponsored by the U.S. Department of Transportation serving the Mountain-Plains Region. Consortium members:

Colorado State University
North Dakota State University
South Dakota State University
University of Colorado Denver
University of Denver
University of Utah
Utah State University
University of Wyoming

Damage Assessment, Characterization, and Modeling for Enhanced Design of Concrete Bridge Decks in Cold Regions

Frank Yazdani, Ph.D., P. E.

Department of Civil and Environmental Engineering
North Dakota State University
Fargo, North Dakota

July 2015

Acknowledgments

The principal investigator gratefully acknowledges all individuals who contributed to the present research report. Special thanks goes to Mr. Ashkan Saboori and Mr. Andrew Reberg for their major contributions. The author also thanks Dr. Mijia Yang, Dr. Denver Tolliver, and Dr. Jimmy Kim for their contribution and insightful discussions.

Disclaimer

ABSTRACT

Concrete has been used in dams, bridges, and highway pavements in which freeze-thaw process and cyclic loading are considered as important factors affecting its mechanical behavior during its service life. Damage caused by frost expansion is a primary concern when designing concrete structures in cold weather regions. It is known that the onset of damage within concrete can be accelerated when a freeze-thaw cycle occurs while a structure is subjected to an external loading. Also, concrete under fatigue loading gradually loses its strength with an increase in the number of load cycles regardless of the loading path (uniaxial or biaxial) and fails under loading significantly less than its strength. The strength reduction and more compliant behavior in concrete are due to widespread micro-cracks that form during freeze-thaw cycles as well as fatigue loading. Under such processes, the mechanical properties such as strength, stiffness, and ultimate strain are affected. In this report, changes in the mechanical properties for concrete and under fatigue loading and freeze-thaw cycles are investigated. Modern theories of damage mechanics with rate independent approach are extended to cover fatigue loading and freeze-thaw cycles. Different softening functions are proposed to predict the mechanical properties of concrete as the number of cyclic loading as well as freeze-thaw cycles increases. The results of the model are compared to the experimental data available in the literature that show a good correlation.

TABLE OF CONTENTS

LIST OF FIGURES

EXECUTIVE SUMMARY

Concrete has been used in various structures due to its unique features such as high compressive strength, good resistance to aggressive and moist environments compared to other construction materials, and enhancement in strength and deformation capacity under confining stresses. This report presents constitutive modeling of concrete after application of fatigue loading as well as freeze-thaw processes. Concrete under fatigue loading gradually loses its strength with an increase in the number of load cycles regardless of the loading path (uniaxial or biaxial) and fails under a loading level significantly less than its strength. In addition, it is widely accepted that concrete shows more flexible behavior under freeze-thaw process as well as fatigue loading due to widespread micro-cracks that accumulate during both conditions. The presence and the formation of micro-defects deteriorate concrete and affects its mechanical behavior such as strength, stiffness, and ultimate strains. In this research report, a rate independent model is presented to cover concrete response to fatigue loading and freeze-thaw cycles. Different softening functions are proposed to predict the mechanical properties of concrete as the number of cyclic loading as well as freeze-thaw cycles increases. The results of the model are compared to the experimental data available in the literature which show a good correlation.

.

1. INTRODUCTION

Concrete is a composite material, which has been widely used as a construction material in many types of infrastructures in the past few decades because it possesses various useful properties. Some of the properties that make concrete a preferable material compared with other materials in construction are as follows: ease of production, economically appropriate, formability to any shape, relatively high compressive strength, and resistance to extreme environmental conditions such as moisture. Concrete is used as the primary material in structures such as dams, bridges, airports/highway pavements, and power plants. Concrete in these structures is generally subjected to different loads such as axial, bending, and torsional loadings, which affect its mechanical behavior and its strength capacity. Therefore, behavior of concrete and changes in its mechanical properties due to the application of various types of loadings are important factors that could have significant impacts on the design of structures. Researchers have attempted to understand the complex behavior of concrete by developing new models. Although various models have been proposed thus far, there is still no comprehensive model that could predict the behavior of concrete thoroughly.

Concrete has some unique mechanical properties compared with other construction materials such as metal. Concrete is almost 10 times stronger under compressive loading than under tensile loading. Its strength and stiffness are dependent on the stress state that concrete is subjected to. One could say that concrete's strength and deformational capacities under biaxial compressive loading are enhanced compared with uniaxial loading. In general, it has been shown experimentally that strength and ductility of concrete increase under confining pressure.

Structural analysis of bridge decks and pavements show that bi-axial stress states are the dominant form of load paths in such structures. Based on such analysis and information, many experimental research efforts have been done on the mechanical behavior of concrete under monotonic and fatigue uniaxial, biaxial, and some triaxial loading and subsequently many theoretical models have been proposed.

Moreover, many bridges and pavements are constructed in regions with extreme cold climates, like North Dakota, where the freeze and thaw process becomes an important factor in influencing the mechanical behavior of concrete. Voids and microcracks are intrinsic parts of the concrete that let the water and moisture enter the concrete. In warm seasons, water and moisture infiltrate the material and fill up the voids and microcracks and, during cold seasons, the entrapped water freezes. The result of this process is the generation of internal hydraulic pressure, which induces tensile stresses inside the concrete microstructure. Since concrete has a low tensile strength; it cracks and additional microcracks and voids are formed letting more water to infiltrate. Repeating these cycles over a period of time would cause damage to increase and the strength of the concrete gradually to decrease to the point where sudden failure due to applied service loads would occur.

Since fatigue loading and freeze-thaw processes are important factors in the design life of concrete in bridges and pavements, the need for a model that could predict the behavior of concrete under these conditions has become more paramount.

This research attempts to develop a rigorous mathematical model based on a class of continuum damage mechanics. In this approach, concrete is a composite material composed of cement paste phase and aggregates. Since it is a non-homogeneous material, its mechanical properties are direction dependent. Concrete under loading shows a nonlinear behavior due to two different microstructural changes. These changes are due to formation of microcracks and occurrence of plastic flow. Microcracks nucleate and propagate upon the application of loads on concrete. Microcracks result in an irreversible process in concrete named damage. Damage is an anisotropic process that depends on the direction in which loads are being applied. The plastic flow, which is not studied in this research, happens when a significant confining pressure state is present. The plastic flow is the dislocation process of aggregates field that occurs along slip planes under internal shear stresses during loading. When the dislocation happens, the number of bonds that are destroyed are the same as the number of bonds that are created. Therefore, in this case no damage occurs to the concrete and consequently no strength and stiffness reduction will occur (Reberg, 2013).

The next section will discuss the mechanical behavior of concrete under different loading paths and freeze-thaw processes. In Section 3, the thermodynamics and damage mechanics concepts will be explained. In Section 4, the literature review will be provided. In Section 5, the new model is proposed in order to predict the stress-strain behavior of concrete under freeze-thaw cycles accurately. The model will be capable of predicting the reduction in modulus of elasticity and increase in the ultimate strain, strain at which failure occurs, as the number of cycles of freeze and thaw (CFT) increases. In Section 6, a new model for concrete under fatigue loading will be developed by incorporating a new factor into the softening function in order to take the effect of mean stress into consideration. Conclusion and future work will be presented in Section 7, followed by a list of references.

2. REVIEW OF MECHANICAL BEHAVIOR OF CONCRETE

2.1 Introduction

To model the behavior of concrete under loading, a thorough understanding of damage processes, which lead to changes in the mechanical properties of the material, is needed. The complexity of concrete characterization has amplified the need for experimental studies. In this section, the effects of monotonic and cyclic multiaxial loading, as well as the freeze-thaw process on the mechanical behavior of concrete, are presented. In order to do so, a literature review has been done on multiaxial experimental tests on concrete for monotonic and fatigue loading followed by an investigation on the influence of CFT on concrete properties. The results have been used to develop two anisotropic models, which could capture the behavior of concrete under fatigue loading with various mean stresses as well as the freeze and thaw process.

The complex behavior of concrete is attributed to its microstructure, which is composed of different phases. The linear or nonlinear behavior of concrete depends on the amplitude of applied loading. Basically, an increase in amplitude of loading would lead to further nonlinearity of concrete behavior. From experimental investigations, it is observed that at stress levels of about 15% to 30% of the uniaxial compressive strength, the occurrence of microcracking results in nonlinear inelastic response (Karnawat, 1997).

However, microcracks are also the intrinsic features of concrete. It means that prior to any external loading, microcracks exist within the concrete. These microcracks could be found in the cement paste and/or at cement matrix/aggregate interface as well (Dhir and Sangha, 1974; Mehta and Monteiro, 2006). By applying loading on concrete, the pre-existing microcracks start to propagate to the cement paste and the ones that already exist in the cement paste would propagate until they reach surrounding aggregates. In addition, new microcracks may nucleate and propagate in the concrete as well. This process continues by increasing the amplitude of loading until a point at which microcracks form a macro scale crack. At this point, the cracks may coalesce and form major cracks, which finally results in material failure.

There are a number of key experimental tests used throughout this research study to calibrate the theoretical model or used to compare with model results. These are summarized here, and include any relevant discussion or observation.

2.2 Behavior of Concrete Under Monotonic Loading

2.2.1 Monotonic Uniaxial Tension

A schematic stress-strain curve for uniaxial tension is shown in Figure 2.1.The stress-strain curve obtained from this experiment is similar to the one obtained from uniaxial compression. The peak stress is designated by f_t, which is known as the tensile strength of concrete. Concrete possesses a relatively low tensile strength compared with its compressive strength. Its compressive strength is almost 10 to 20 times greater than its tensile strength. This could be attributed to the different processes of nucleation and propagation of microcracks under tension versus compression. In tension, microcracks nucleate and propagate in the perpendicular

direction to the loading and result in splitting the specimen in relatively short intervals, as seen in Figure 2.2. By increasing microcracking, the available load-carrying area decreases, which results in an increased stress concentration close to the tip of the cracks. As a result, the cracks coalesce together and lead to material failure.

For stress amplitude less than 60% of tensile strength, the nucleation and propagation of microcracks are quite small and the stress-strain behavior of concrete is approximately linear. But as the stress amplitude reaches 75% of the ultimate strength, the microcracks propagation becomes significant, resulting in a nonlinear stress-strain behavior. As more microcracks form upon further loading of the concrete, the strain increases. It could be noticed that the stiffness of material E decreases with increasing the strain, demonstrating the effect of microcracks and damage on the modulus of elasticity (Evans and Marathe, 1968). Upon unloading the concrete, there is always irreversible deformation present, which is called inelastic damage. This inelastic strain is due to irrecoverable damage occurred in concrete (Gopalaratnam and Shah, 1985; Reinhardt *et al.*, 1986).

Uniaxial tensile strength, f_t, ultimate (failure) tensile strain, ε_u, Young's modulus, E_0, and Poisson's ratio, ν, are some of the mechanical material properties that could be obtained from uniaxial tension experiment.

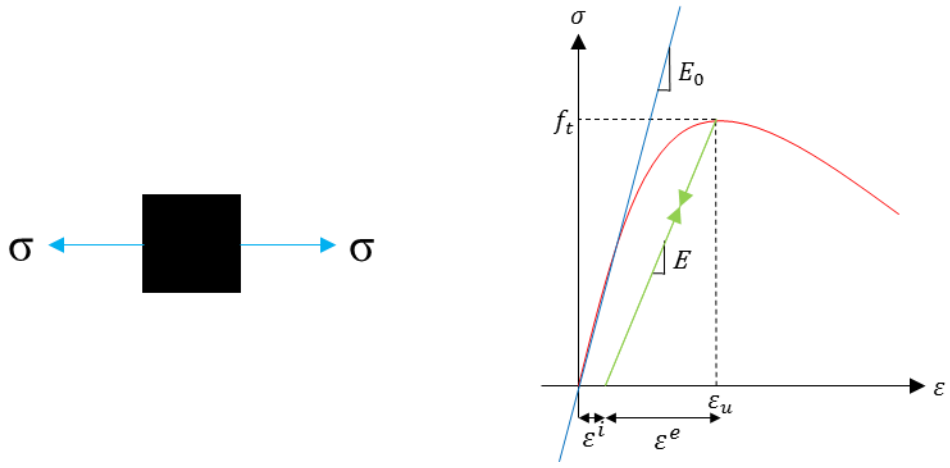

Figure 2.1 Schematic stress-strain curve for uniaxial tension

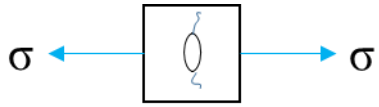

Figure 2.2 Microcracks nucleation pattern under uniaxial tension

2.2.2 Monotonic Uniaxial Compression

Monotonic uniaxial compression test is the most common test carried out on concrete specimens. This test could be carried out either on cylindrical or cubic specimens. Figure 2.3 shows a schematic stress-strain curve for uniaxial compression. The peak stress point on the curve is denoted as f_c, which represents the compressive strength of concrete. In general, the test could be

run at an imposed stress rate or an imposed displacement rate with the latter allowing the post-peak regime of the response to be obtained (Torrenti et al., 2010). The stress-strain curve obtained from the uniaxial compression test can be considered to be composed of several regions. At early stages of loading, at which stress does not exceed 30% of compressive strength, concrete displays a linear relation between stress and strain, indicating that microcracks are unaffected by loading. In other words, the pre-existing microcracks normally do not propagate and new microcracks do not form at this stage. At stress levels between 30% and 50%, concrete shows nonlinearity in its stress-strain behavior. In this range, the stress at the interface of aggregates and the cement paste reaches the interfacial bond strength between them and results in formation of new cracks at the interface. Microcracks do not, however, propagate into the matrix paste since matrix paste has a higher fracture toughness. The third stage occurs when the stress level is between 50% and 75% of compressive strength. At this stage, cracks appear and propagate into the mortar matrix. Stress redistribution occurs and as a result the stiffness of material is reduced and the material becomes more compliant. In the fourth stage, at which the stress level is greater than 75% of compressive strength, the cracks continue to nucleate and propagate at a greater rate. These cracks start to coalesce and form bigger cracks and consequently reduce the load-bearer section of the material. Finally, at a specific point concrete loses all its strength and fractures abruptly.

The last part of stress-strain curve is the descending branch of the behavior following the peak point and is called strain softening. This part depends on various factors such as loading rate, stiffness characteristics of the loading machine, size of the test specimen, localization of the microcracks, etc. (Karnawat, 1997). Many researchers have claimed that the softening part is structural dependent rather than material dependent (Van Mier, 1984; Pijaudier-Cabot and Bazant, 1987; Schreyer, 1995). For concrete, the ultimate strain (strain at which failure occurs) under compressive loading is greater than the one under tensile loading. This could be attributed to the microcracks formation type (damage), which is different for each of the loadings. Modeling of the softening behavior of concrete that considers localization is beyond the scope of this research and will not be considered.

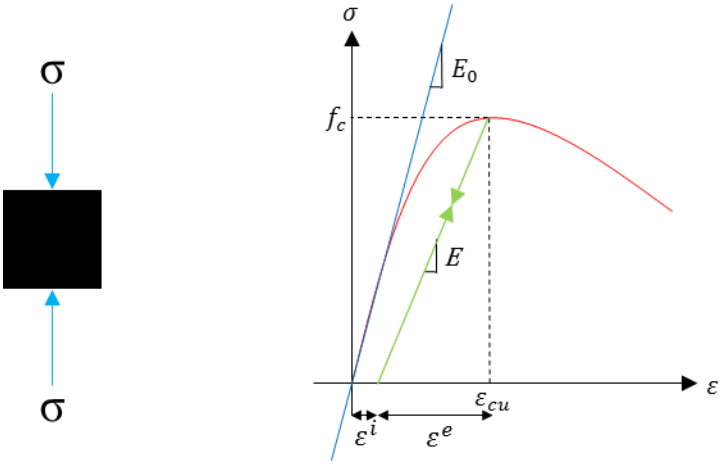

Figure 2.3 Schematic stress-strain curve for uniaxial compression

Microcracks formed during the processes of compressive loading alter the mechanical properties of concrete such as Young's modulus, E_0, and Poisson, ν. Many researchers have investigated the type of

crack formation due to uniaxial compression and concluded that the microcracks are formed parallel to the direction of the applied load. This type of crack formation is referred to as mode-II type cracks (Wastiels, 1979; Ashby and Amp, 1986; Horii and Nemat-Nasser, 1986). At the crack interfaces, shear stresses cause shear sliding and crack separation, Figure 2.4.

Figure 2.4 Microcracks nucleation pattern under uniaxial compression

When the stress level exceeds the point at which microcracks appear in concrete and damage occurs, permanent deformation will be generated. The permanent deformation, also referred to as inelastic strain, is due to misfit of crack faces or development of a crack tip process zone (Krajcinovic, 1985). Also, it is observed that the slope of the unloading curve is not the same as the initial slope of stress-stain curve, which represents the initial modulus of elasticity and is due to the degradation occurred because of nucleation and propagation of microcracks into the concrete.

2.2.3 Monotonic Biaxial Compression

Biaxial stress state represents the condition at which concrete is under loading in two orthogonal directions. To design structures such as pavements, bridges, shells, and plates, a study of biaxial stress on concrete is required. It has been reported by several researchers that concrete shows enhancement in both stress and strain behavior under biaxial compression. The strength enhancement of concrete under biaxial compression depends on the biaxial stress ratio $\frac{\sigma_1}{\sigma_2}$. Figure 2.5 shows the compressive strength of concrete under different load paths presented by (Lee et al., 2004). One can see that the maximum strength of concrete under compressive loading is at the stress ratio of 0.5. It could be seen from the experimental data that the strength of concrete under this load ratio increases about 20% to 30% of its uniaxial compressive strength.

Concrete under biaxial compression also shows more ductile behavior than uniaxial compression due to the more confining effects of pressure. Under uniaxial compression, microcracks form more or less parallel to the direction of loading and the crack opening occurs in the perpendicular direction to loading. Under biaxial compressive state, with the addition of a confining load in an orthogonal direction, crack opening is inhibited such that it requires larger loads to cause a crack to form. As a result, concrete under biaxial compression displays more strength and ductile behavior than during uniaxial compression. Figure 2.6 shows the stress-strain behavior of concrete under various biaxial stress ratio as well as uniaxial provided by Shang and Song (2006). In this figure, the horizontal axis represents the strain and the vertical axis represents the normalized stress with respect to uniaxial strength of concrete. The symbol ξ is the stress ratio

(ratio of vertical stress to horizontal stress). This figure confirms the features discussed before about the behavior of concrete under multiaxial loading. It can be observed that the strength and deformational capacity of concrete increases by increasing stress ratio as confining pressure is provided.

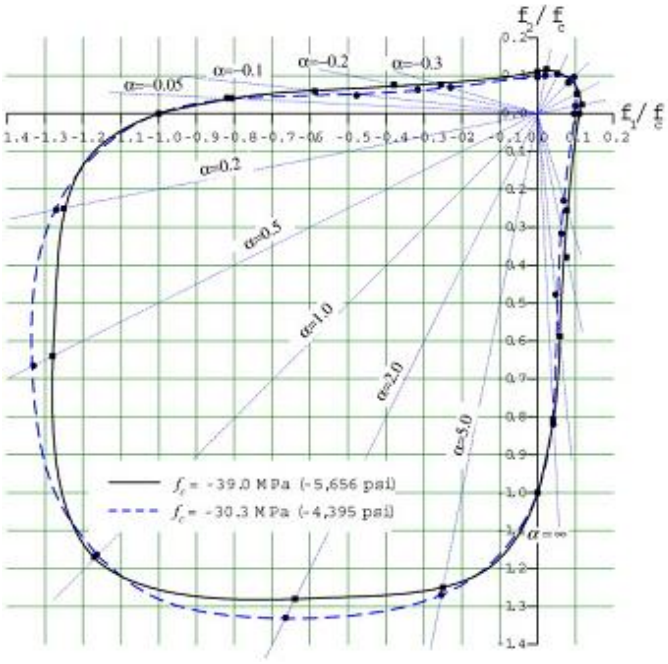

Figure 2.5 Biaxial strength envelope of concrete (Lee et al., 2004)

2.2.4 Monotonic Biaxial Tension

Microcracks propagation in biaxial tension is not inhibited as it is in compression. Therefore, microcracks propagate rapidly and form major cracks leading to a sudden rupture. Concrete behaves in the same way as in uniaxial tension and its ultimate strength is almost the same as its uniaxial tensile strength. It has been reported that the failure behavior of concrete under biaxial tension is the same as its behavior under uniaxial tension. In other words, a failure plane perpendicular to the direction of the largest tensile stress is formed (Kupfer et al., 1969). Krajcinovic (1985) argues that, however, the crack propagation is even more unstable in the biaxial tension loading than uniaxial loading.

2.2.5 Monotonic Biaxial Tension-Compression

Concrete under biaxial tension-compression shows less compressive strength than under uniaxial compression. Concrete behavior under this type of load state is a transition from behavior under uniaxial compression to behavior under uniaxial tension. When the magnitude of tensile loading decreases, the concrete stress-strain behavior is more like its behavior under uniaxial compression. By increasing the tensile stress level, cracks occurring in the perpendicular direction of loading influence the behavior of the material.

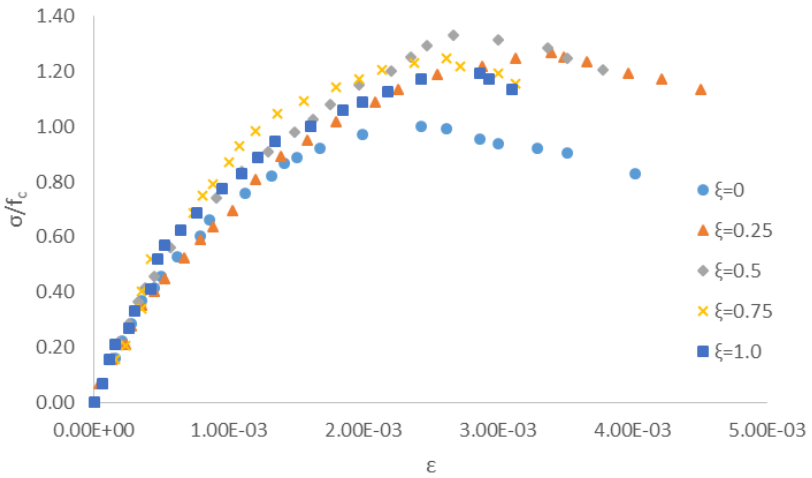

Figure 2.6 Stress-strain curves of concrete under uniaxial and biaxial loading, data by Shang and Song (2006)

2.3 Behavior of Concrete Under Fatigue Loading

Fatigue is a process of deterioration of a material under repeated loading. This deterioration is generally due to nucleating and propagating of microcracks, which progress with the number of applied loading cycles. This irreversible process changes the mechanical properties of the material and leads to the failure at a level of loading much lower than the material static strength.

Figure 2.7 shows the schematic stress-strain curve of concrete under fatigue loading as well as monotonic loading. As shown in the figure, f_c is the static strength of concrete, ε_u is the monotonic failure strain, σ_{max} is the maximum fluctuating stress of cyclic loading and also is the stress at which failure will occur after a specific number of cycles, σ_{min} is the minimum fluctuating stress, which is zero in this case, $\Delta\sigma$ is the stress range (σ_{max-} σ_{min}), ε_{min} is the strain corresponding to the minimum fluctuating stress, ε_{max} is the strain corresponding to the maximum fluctuating stress, and ε^f_u is the cyclic failure strain. It is observed that irreversible strain will be accumulated after each cycle due to the occurrence of microcracks during the fatigue process. Therefore, the material becomes more compliant under fatigue loading and as a result, failure strain becomes greater than the failure strain under monotonic loading as shown in Figure 2.7.

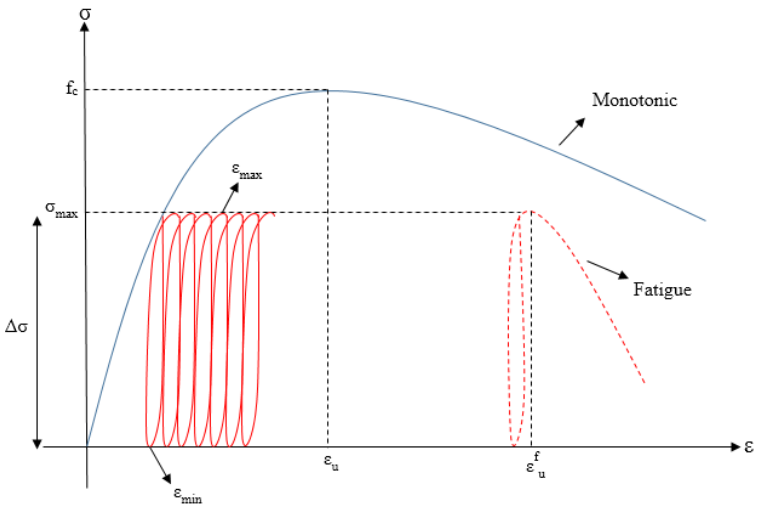

Figure 2.7 Schematic representation of stress-strain diagram of concrete under fatigue and monotonic loading

Generally, microcracks formed during the process of fatigue have the same nature as the ones formed under static loading. However, microcracks are more numerous and more widely spread under the cyclic loading than under the static loading. Fatigue microcracks occur around the aggregates and in the mortar matrix. Similar to the case of static loading, the favored direction of microcracks formation under compression is parallel to the direction of loading, and for the case of tensile loading it is perpendicular to the loading direction.

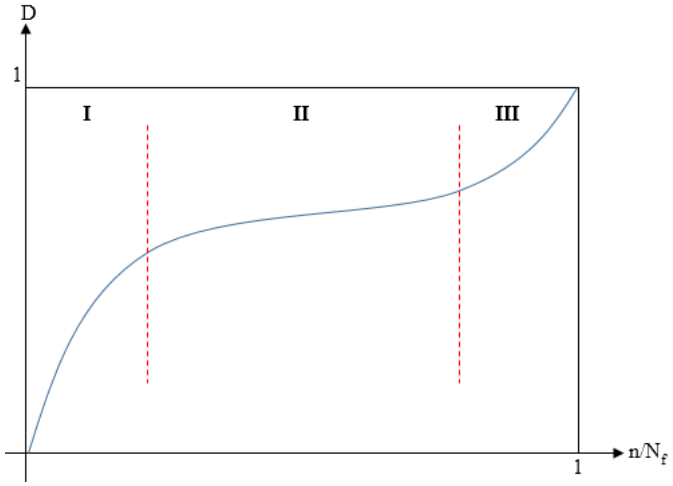

Figure 2.8 Damage accumulated versus fatigue life ratio

Fatigue microcracking is a progressive irreversible phenomenon that deteriorates the inner structure of the material. Damage that occurs during the fatigue process in concrete is known to consist of three stages. Figure 2.8 is a schematic representation of damage occurring during the cyclic loading. In this figure, vertical axis, shown as D, represents the damage in the material that occurred during the process of fatigue loading and horizontal axis, shown as n/N_f, represents the ratio of number of cycles of loading to number of cycles to failure. It shows the existence of three phases in the process of the fatigue of concrete: 1) the initial phase, during which damage

occurs in the concrete at a higher rate as pre-existing cracks in the interface zone propagate until they reach a stable phase. This phase covers about 5% to 10% of the whole fatigue life of concrete. 2) the second phase, during which the rate of damage is stabilized corresponding roughly to the plateau part of the graph shown in Figure 2.8. It is thought that at this phase the stronger mortar phase arrests the rapid propagation of the interface cracks. This part covers up to 80% to 90% of the whole fatigue life of concrete. 3) the final phase, during which the rate of damage is progressively accelerated due to the propagation of unstable cracks and finally leads to failure. This part constitutes almost 5% to 10% of concrete fatigue life. The same behavior for strain is reported by Song et al. (2005), which is shown in Figure 2.9.

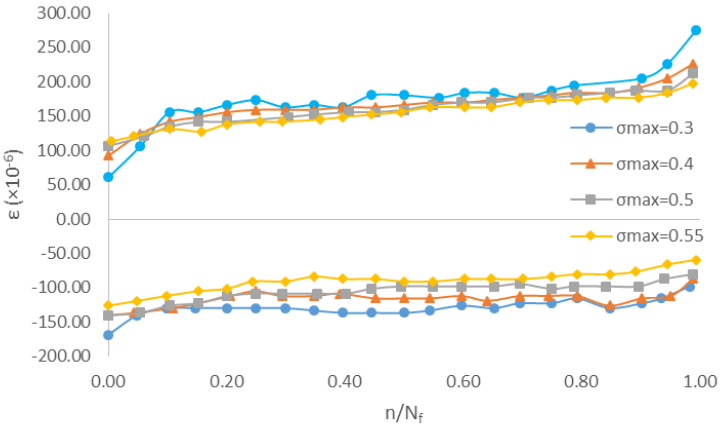

Figure 2.9 Strain versus fatigue life ratio, data by Song et al. (2005)

One of the most common ways to represent the fatigue data of concrete is S-n curves. In this type of curve, y-axis represents the strength of the material and x-axis represents the number of load cycles. Consequently, each data point on the curve denotes the fatigue life of the material under a specific stress level. Concrete under cyclic loading loses its strength gradually with an increase in the number of load cycles no matter if the loading is uniaxial or multiaxial. During the cyclic loading, microcracks nucleate and grow to a stage at which they coalesce and form major cracks that reduce the carrying load section tremendously. At this point, the strength of the material has decreased and becomes equal to the amplitude of the cyclic loading, which will cause a sudden rupture in the material. It has been argued that at any given cycle, the fatigue strength of concrete under biaxial compression is greater than that under uniaxial compression (Su and Hsu, 1988; Lu et al., 2007). This is the result of the confinement provided in the biaxial loading state. This confinement restricts the nucleation and propagation of microcracks by applying load in the perpendicular direction. Figures 2.10 – 2.12 show S-n curves for various load paths presented by Yin and Hsu (1995). Fatigue tests are generally very scattered. In the case of concrete, the fatigue life for a given stress level may vary in the ratio of 1 to 100. Therefore, the fatigue strength is not defined by one single average value. A correct representation must include a notion of probability (Holmen, 1982; Siemes, 1982; Yang, 1994).

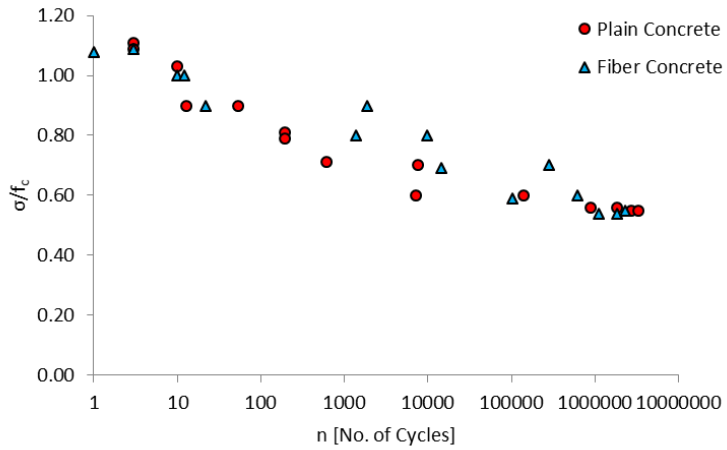

Figure 2.10 S-n curve of plain and fiber concrete under uniaxial compression, data by (Yin and Hsu, 1995)

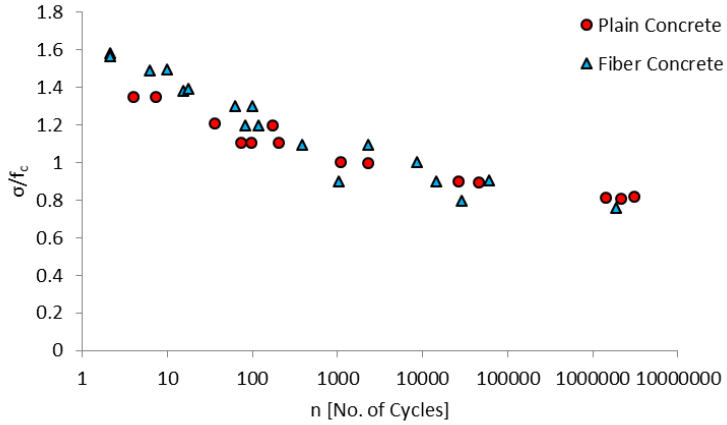

Figure 2.11 S-n curve of plain and fiber concrete under biaxial compression with stress ratio of 0.5, data by Yin and Hsu (1995)

In addition to strength reduction, cyclic loading affects the modulus of elasticity and deformation capacity of concrete as well. Awad (1971) and Gao and Hsu (1998) have investigated the effects of fatigue loading on ultimate strain of concrete (strain at which failure occurs) and concluded that this strain increases under the cyclic state compared with the one under monotonic state. Figure 2.13 shows the increase in failure strain by increasing the number of cycles to failure. Each data point on the graph represents a specific fatigue loading with different amplitude. The data on the graph, from left to right, correspond to the monotonic and fatigue loading with the maximum fluctuating stresses of 0.95, 0.9, 0.85, and 0.5, respectively. Awad (1971) has concluded that ultimate strain and irreversible strain, accumulated after each cycle prior to failure, depend on the number of cycles that load is being applied.

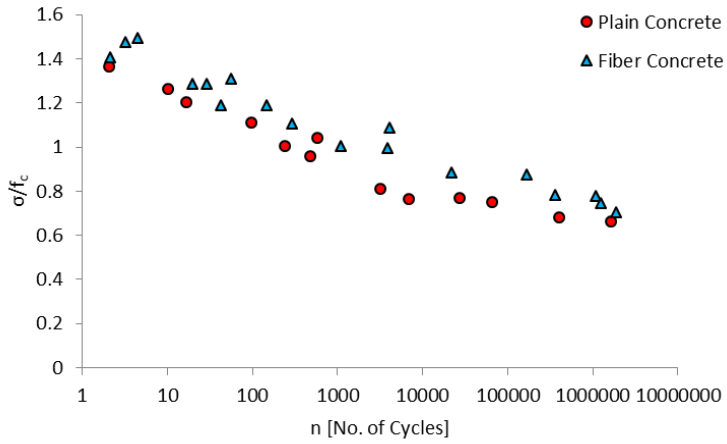

Figure 2.12 S-n curve of plain and fiber concrete under equal biaxial compression, data by Yin and Hsu (1995)

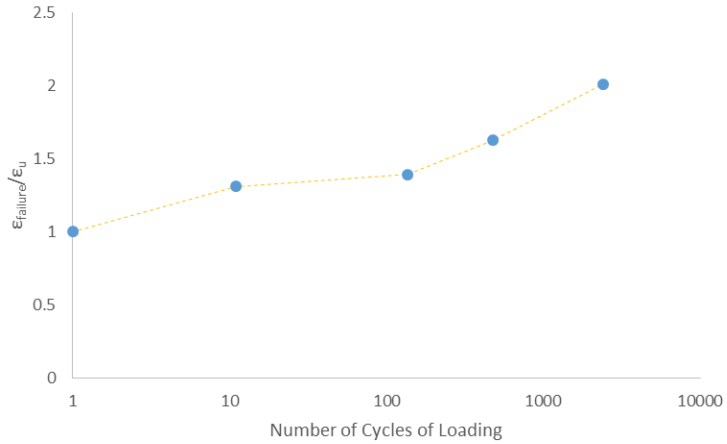

Figure 2.13 Failure strain versus number of cycles to failure, data by Awad (1971)

In addition to maximum stress, Aas-Jakobsen and Lenschow (1973) and Hsu (1981) have shown that stress range also has significant effects on the fatigue life of concrete. In order to show the stress range influence on fatigue life, the term stress ratio R is used. R is the ratio of minimum fluctuating stress to maximum fluctuating stress. The range of R is between 0, corresponding to minimum fluctuating stress of zero, to 1, corresponding to sustained loading at which the maximum and minimum fluctuating stresses are the same. Figure 2.14 schematically shows the effect of R on the fatigue life in the S-N diagram. It has been shown that by keeping the maximum stress unchanged and decreasing the stress range (increasing R), the number of cycles to failure will increase. Therefore, maximum stress and stress range are the factors that affect the ultimate and irreversible strain. These results have been investigated by Awad (1971) and their validation has been shown.

Gao and Hsu (1998) have argued that the fatigue strain of concrete comprises three parts: irreversible strain caused by cyclic creep under the action of average stress; irreversible strain caused by fatigue cracks; and fatigue strain range. Also, Gao and Hsu (1998) have reported that the modulus of elasticity of concrete degrades during the fatigue process due to damage accumulation as a result of microcracking.

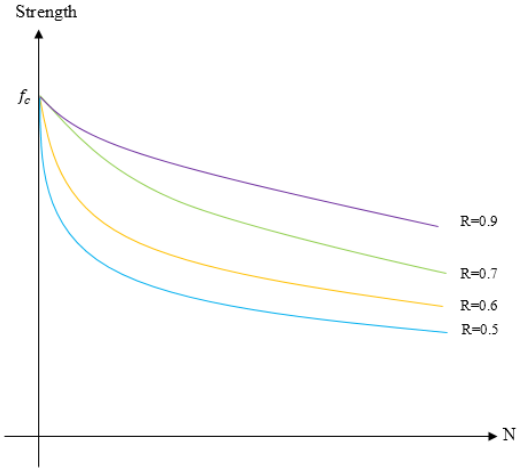

Figure 2.14 Schematic representation of S-N curves for various values of R

The fatigue behavior of concrete depends on the characteristics of the material, the type and level of loading, the frequency and shape of the cycle, and the environmental conditions. In fact, the fatigue strength of concrete depends on the same parameters that affect its static strength such as nature and type of the aggregates, aggregate mixture grading, proportion of cement, water to cement ratio, porosity, and method of casting and curing (Raithby and Galloway, 1974; Klcriber, 1982; Petkovic et al., 1990; Kim and Kim, 1996; Ahmed et al., 1999). In addition to the material parameters, concrete fatigue strength also depends on the loading specifications such as amplitude of stress, mean stress, stress range, load path (biaxial stress ratio), and loading frequency (Antrim and Mclaughlin, 1959; Assimacopoulos et al., 1959; Karsan and Jirsa, 1969; Tepfers and Kutti, 1979; Hsu, 1981; Qiao and Yang, 2006). The effects of first three will be discussed when the model is demonstrated. The description of the fatigue loading contains two time-related parameters, namely the frequency and the shape of the cycle. The influence of these two factors are moderate in the case of low-level cyclic loading at which the maximum stress level is less than 80% of the static strength.

In the case of concrete, for higher level of loading, the process of damage is governed by the duration of process more than its cyclic nature. It has not been established yet whether concrete exhibits fatigue limit.

The S-N curves introduced previously are established just for the case of identical loading cycles. In reality, fatigue loading consists of cycles of loading with various amplitudes and stress ranges. To predict the fatigue life of concrete due to variable cyclic loading, two solutions have been proposed; rule of linear accumulation and rule of non-linear accumulation. These methods consist of quantifying the evolution of fatigue process by means of a rule of damage accumulation. The most common method used for the linear cumulative damage is Palmgren-

Miner (Miner, 1945). Figure 2.15 is an illustration of the linear Palmgren-Miner law for the amount of damage accumulated in the concrete due to fatigue loading. In these figures, S represents the strength of the material, N_F is the number of cycles of loading to failure, D is the damage occurred in the material due to cyclic loading, and δ is the ratio of number of cyclic loading to the number of cycles of loading to failure.

An efficient model, which could capture the behavior of concrete, is needed because fatigue loading has a significant influence on concrete serviceability, and that concrete failure under this loading condition is an abrupt phenomena with serious consequences.

2.4 Freeze-Thaw Process

In recent years, studying the freeze-thaw processes on concrete has developed considerably due to its significant effects on mechanical properties of concrete such as stiffness, deformation capacity, and strength. Concrete is a porous material that can absorb water and moisture into its intrinsic pores and previously formed shrinkage cracks. Therefore, concrete is a material susceptible to freeze-thaw processes and its mechanical properties deteriorate during this process. The amount of water absorbed by concrete depends on different parameters such as concrete mixture proportions, degree of saturation, presence of chemical admixtures, physical characteristics of the cement and aggregates, and its air contents. Basically, the freeze-thaw process can be thought of as a complex form of fatigue loading. The damage occuring due to freeze-thaw process into the concrete could be accelerated in the presence of significant external loading (Miao *et al.*, 2002).

Damage occurred in the concrete during the process of freeze-thaw could be categorized into three types explained in the following sections.

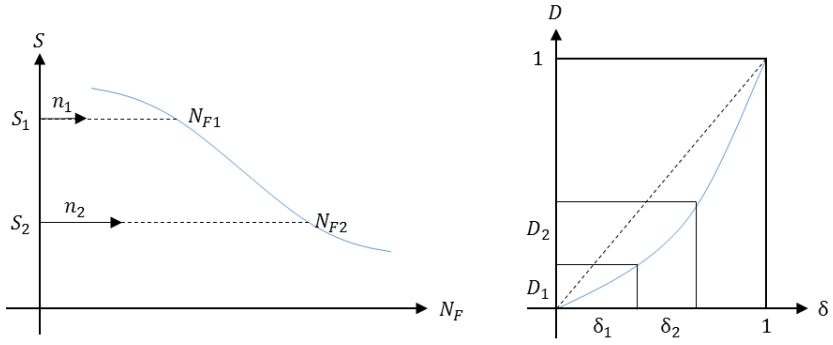

Figure 2.15 Illustration of the linear Palmgren-Miner law

2.4.1 Types of Freeze-Thaw Damages in the Concrete

2.4.1.1 D-cracking

D-cracking is a form of concrete deterioration due to the freeze-thaw process associated with the use of coarse aggregates that disintegrate when they become saturated. Typically, D-cracking occurs around joints and edges of pavement where concrete is exposed to wet and dry cycles at both the top surface and sides of slab. In addition, curling and warping would induce stress

concentration at corners and edges of the concrete slab, making this region of slab more susceptible to D-cracking. Figure 2.16 shows the D-cracking in concrete pavement due to freezing-thawing.

Figure 2.16 D-cracking in concrete pavement (picture from www.civildigital.com)

2.4.1.2 Crumbling

Crumbling or scaling is a type of concrete deterioration occuring because of the freeze-thaw process. It appears as a separation of a thin layer of the top surface from the body of concrete. The separated thin brittle layer then crumbles under traffic and leaves underneath aggregates exposed. Parts of concrete exposed to ponds of water and salt solution or continuous wetting are susceptible to this type of damage. Figure 2.17 illustrates various examples of crumbling in concrete sidewalks.

Figure 2.17 Crumbling in concrete (picture from www.greenpiece1.com)

2.4.1.3 Internal Cracking

Hydraulic pressure and ice accretion are two mechanisms that cause internal damage in concrete (Detwiler et al., 1989). As mentioned earlier, water and moisture exist in concrete's voids and pores. As temperature drops below 0° C, water in capillary pores freezes and expands almost 8% to 9% of its water phase volume. If the required space due to expansion is more than the space provided by the pores and voids of concrete, the excess volume of frozen water induces hydraulic pressure on the cement paste. The magnitude of this hydraulic pressure depends on the permeability of the cement paste, the degree of saturation, the distance to the nearest unfilled void, and the rate of freezing. If the induced pressure exceeds the tensile strength of the cement paste at any point, it will cause local cracking at that point. Afterward, during the thawing portion of this process, more water enters the cracks; by repeating this cycle, deterioration in concrete progresses. This process typically does not occur at relatively low freezing rates.

In the case of low freezing rate, the hydraulic pressure is not great enough to damage the cement paste, but still, pressure may be produced because of ice accumulation in the capillary pores. According to Cordon (1966), water in the gel pores freezes at almost -78° C. This is due to the small radius of gel pores that form strong surface tension forces applied on the surface of the water. Therefore, when the temperature drops below 0 °C, the water in the gel pores remains in a liquid state but becomes supercooled. Since it has a higher free energy than the ice in the capillaries, it moves from gel pores into the capillaries where it is more likely to freeze (Detwiler et al., 1989). As a result, the volume of concrete in the form of gel pores decreases and the volume of the capillaries increases due to expansion of water. During the thawing process, some of the water returns to the gel pores, but the original state of the material will not be obtained as this process is not reversible.

2.4.2 Making Durable Concrete to Freeze-Thaw Process

Thus far, it has been pointed out that concrete is susceptible to cycles of freeze-thaw. Its mechanical properties deteriorate gradually as the number of freeze-thaw cycles increases. In order to improve the concrete resistance to freeze-thaw cycles, different approaches could be utilized, and which will be discussed in the following section (Detwiler et al., 1989).

2.4.2.1 Air Entrainment

There are two kinds of air bubbles in concrete: entrapped and entrained. Entrapped air bubbles are unintentionally generated into the cement paste during the process of mechanical mixing, whereas entrained air bubbles are intentionally incorporated by adding chemical admixtures.

The factor that has the most influence on the durability of concrete in the freezing and thawing process is providing a system of well-distributed entrained air voids in concrete. It is believed that entrained air voids reduce the hydraulic pressure by providing free space for frozen water to flow through. Induced hydraulic pressure due to the freeze-thaw process increases with distance from a void. The magnitude of hydraulic pressure is less than the tensile strength of cement paste in the specific radius of air voids. The enclosed zone by this radius could be assumed the protection zone for the cement paste. Therefore, in order to reach this protection zone all over the cement paste, a system of well-distributed air voids is needed. As result, during freezing time, ice can accumulate in the air voids without building up excessive pressure. The maximum acceptable air-void spacing factor recommended by ACI is 200 μm.

2.4.2.2 Water-Cement Ratio

Decreasing the water-cement ratio has a significant influence on the freeze-thaw durability of concrete. A low water-to-cement ratio makes a cement paste with higher tensile strength that can better withstand the pressure imposed by hydraulic pressure. Furthermore, a lower water-cement ratio will cause less initial freezable water in the concrete voids. Finally, a lower water-cement ratio decreases the permeability of concrete, which is an advantage in moist environments where water will enter the concrete. Therefore, the lower the permeability, the longer it takes to reach the critical level of degree of saturation.

2.4.2.3 Aggregates

Like cement paste, aggregates absorb water and may be subject to hydraulic pressure. Aggregates that absorb enough water and reach the critical degree of saturation may expand due to frozen water expansion. Unlike cement paste, aggregates possess high tensile strength; therefore, they may not fracture, but their expansion will cause distress in the surrounding paste, which results in cement paste deterioration.

2.4.2.4 Curing

Another factor that affects the concrete durability is curing. The greater the degree of hydration, the less freezable water in concrete pore structures and the higher the tensile strength of cement paste. Adequate time for curing will let the pore structures in concrete to be well spread out. In addition, if the concrete sufficiently dries out during the process of curing, it will be less susceptible to freeze-thaw damage.

2.4.3 Freeze-Thaw Durability Estimation Test

The most common test used to estimate the durability of concrete under freeze-thaw cycles is ASTM C 666, "Resistance of Concrete to Rapid Freezing and Thawing." This test could be done through two different procedures to determine the effects of variations in both properties and conditioning of concrete in resistance to freezing and thawing cycles. In procedure A, rectangular prisms of concrete are frozen and thawed in water; in procedure B, specimens are frozen in air and thawed in water. In each cycle of freeze-thaw, the specimens will be cooled from 40° to 4° F and then warmed to 4° F within two to five hours. In the end, relative dynamic of modulus of elasticity and durability factor will be calculated. In addition, two other tests, ASTM C 671, "Critical Dilation of Concrete Specimens Subjected to Freezing" and ASTM C 682, "Evaluation of Frost Resistance of Coarse Aggregates in Air-Entrained Concrete by Critical Dilation Procedure," are being used to determine the durability of concrete. None of the tests mentioned are intended to provide a quantitative measure of the length of the service of concrete.

2.4.4 Mechanical Changes in Concrete due to Freeze-Thaw Processes

In order to quantitatively investigate the effects of freeze-thaw processes on mechanical properties of concrete, several research studies (Hasan et al., 2004; Shang and Song, 2006; Hasan et al., 2008; Shang et al., 2008; Duan et al., 2011; Liu and Wang, 2012) have been done on concrete. These studies have reported similar results obtained from experiments run on concrete under freeze-thaw. Shang and Song (2006) investigated the stiffness, strength, and deformation performance of concrete after 25, 50, and 75 freeze-thaw cycles subjected to biaxial compression.

Experimental data reported by Shang and Song (2006) show that concrete loses its strength by applying freeze-thaw cycles. Figure 2.18 illustrates the effects of freeze-thaw cycles on the strength of concrete under various load paths. Loading in direction 3, σ_3 is the primary loading direction while σ_2 is the lateral loading. As Figure 2.18 shows, the strength of concrete, regardless of the load path, decreases due to microcracks formed during the freeze-thaw process.

Likewise, it can be inferred from experimental data that the rate of decrease in strength is not the same for different load paths and is path dependent. The highest rate is for uniaxial loading while the lowest is for biaxial with a stress ratio of 0.75. Similar results were reported for concrete under triaxial loading state by Shang et al. (2008). Shang and Song (2006) emphasized that confining loads reduce the damage caused by freeze-thaw cycles. They also claimed that the effect of freezing and thawing cycles on plain concrete does not change the failure mode under biaxial compression. It means that damage mode occurred in the form of crack opening and shear sliding under compressive loading will remain unchanged after cycles of freeze and thaw are applied.

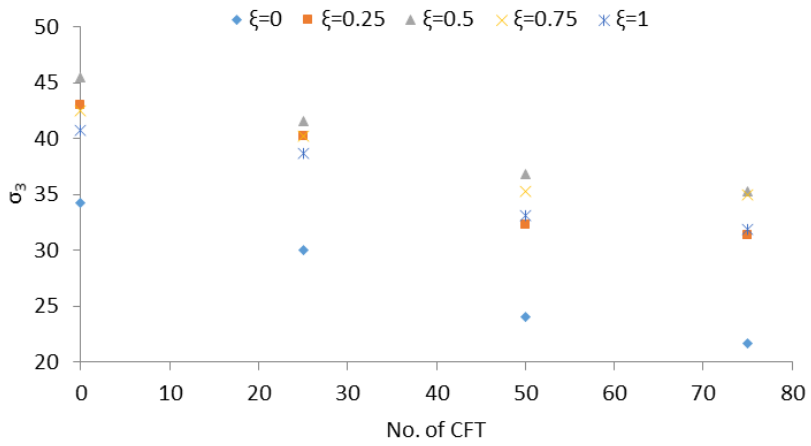

Figure 2.18 Strength versus number of CFT for various load paths, data by Shang and Song (2006)

A similar conclusion could be drawn for deformation characteristics of concrete under freeze-thaw cycles by studying the experimental data reported by Shang and Song (2006). The influence of freeze-thaw cycles on the principal ε_3 under biaxial compression for various load paths is shown in Figure 2.19 by Shang and Song (2006). It could be seen from Figure 2.19 that the principal strains ε_3 under biaxial compression with the same stress ratio increases as the freeze-thaw cycles are applied. This could be attributed to the formation of microcracks during the process of freeze-thaw, which result in the concrete being more compliant and having a higher strain failure. One can note that the principal strain under biaxial loading state is greater than that under uniaxial loading for the same number of freeze-thaw cycles. This shows that concrete behaves more ductile under biaxial compressive loading than uniaxial loading due to the occurrence of crack opening in the perpendicular direction for uniaxial compressive loading. In the case of biaxial loading, crack opening in the perpendicular direction to loading is inhibited by the opposing compressive load in the corresponding direction. It also should be noted that the rate of increase in ultimate strain due to freeze-thaw cycles depends on the load path applied on the concrete. This rate is higher for biaxial loading than uniaxial.

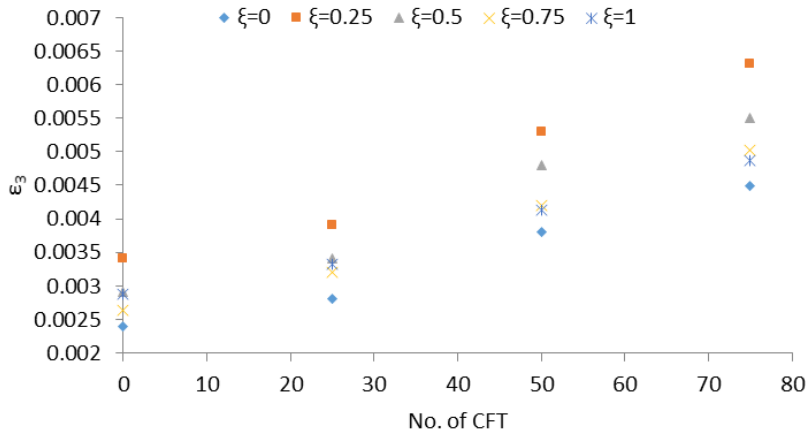

Figure 2.19 Ultimate strain versus number of CFT, data by Shang and Song (2006)

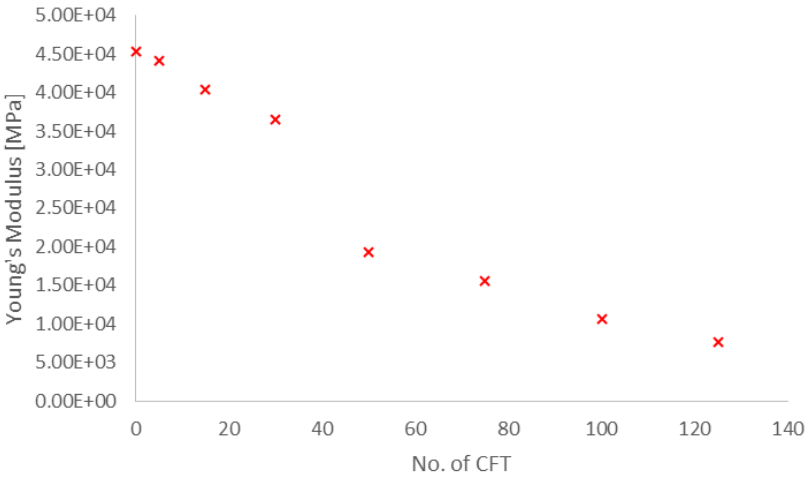

Figure 2.20 Young's modulus versus number of CFT, data by Liu and Wang (2012)

According to the data published by Shang and Song (2006) and Liu and Wang (2012), modulus of elasticity of concrete decreases as the cycles of freeze-thaw increase. Figure 2.20 illustrates the experimental data obtained by Liu and Wang (2012) for changes of modulus of elasticity by applying freeze-thaw cycles . When freeze-thaw is applied on a concrete specimen, new cracks nucleate and propagate into the concrete. By repeating this process, more cracks will be generated while the existing cracks becomes larger. As a result, concrete becomes softer and its modulus of elasticity decreases.

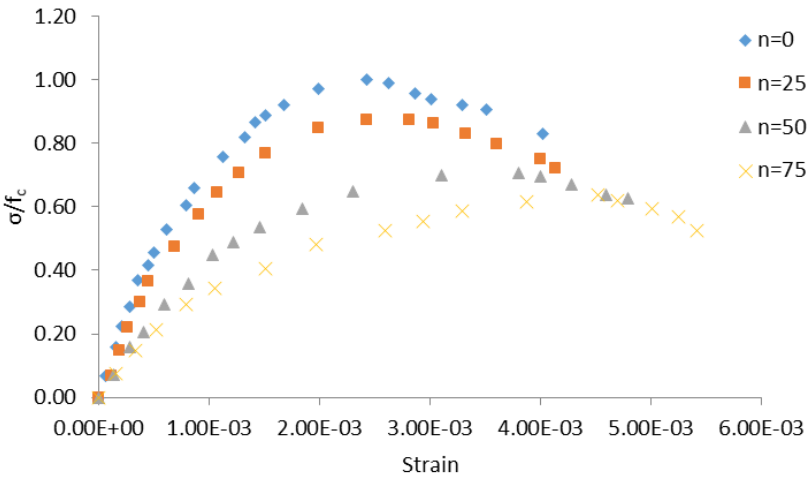

Figure 2.21 Stress-strain curves after freeze-thaw under uniaxial loading, data by Shang and Song (2006)

As a result, it could be noticed that freeze-thaw has a significant influence on strength, deformation, and stiffness of the concrete. Based on the experiments done by Shang and Song (2006), all these effects could be summarized in the stress-strain curves of the concrete after freeze-thaw cycles. Figures 2.21 – 2.23 show the stress-strain curves of concrete under various load paths after different number of cycles of freeze-thaw. These figures show that the freeze-thaw process decreases the strength of the concrete by developing new microcracks into the material. Also, it can be observed from the figures that the ultimate strain of the concrete increases by applying freeze-thaw cycles. A decrease in strength and increases in flexibility depend on the number of cycles of freeze-thaw applied. As the number of freeze-thaw cycles increases the strength decreases while ultimate strain increases.

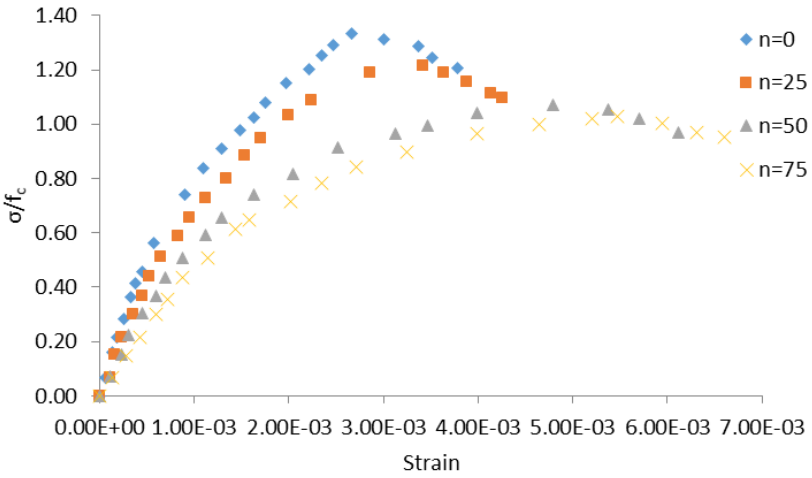

Figure 2.22 Stress-strain curves after freeze-thaw under biaxial loading with ratio of 0.5, data by Shang and Song (2006)

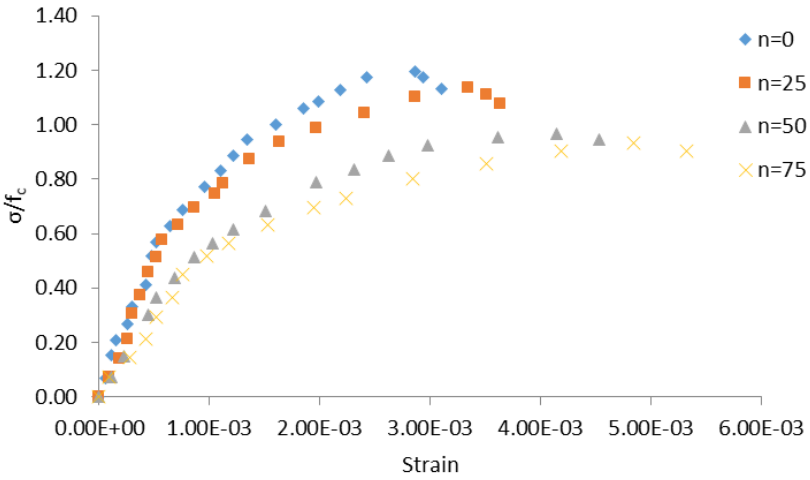

Figure 2.23 Stress-strain curves after freeze-thaw under biaxial loading with ratio of 1, data by Shang and Song (2006)

3. THERMODYNAMICS AND DAMAGE MECHANICS

3.1 Introduction

Thermodynamics is a branch of science used to describe the thermodynamical processes of a system such as mechanical, electrical, and chemical in equilibrium and relate properties to the changes in the energy of the system. Processes in thermodynamics are reversible and irreversible. The reversible processes related to solid mechanics are the ones with perfectly elastic deformation. In a reversible process, a single kinematic variable could be used to describe the state of a solid material by relating the stresses and strains. However in real cases, the solid material will experience inelastic deformation, which is counted as an irreversible process. In order to describe the state of the material under such processes, a single variable will not be sufficient. Therefore, a set of variables will need to be defined in order for the changes in material due to irreversible processes to be captured.

The approach of the thermodynamics of irreversible processes is used in this research. In the following, the formulation will be cast within the framework of the internal variable theory of thermodynamics (Coleman and Gurtin, 1967; Kestin and Rice, 1969; Lubliner, 1972; Krajcinovic and Fonseka, 1981; Truesdell and Baierlein, 1985) and continuous damage mechanics is used to describe the damage occurred within concrete during loading. Also, concrete is assumed to be rate-independent and a single phase material that could be modeled as a continuum.

3.2 Cauchy's First Law of Motion

The total force acting on a continuum body is assumed to be composed of a body force $\boldsymbol{f}_b$ and a contact force $\boldsymbol{f}_c$:

$$\boldsymbol{f} = \boldsymbol{f}_b + \boldsymbol{f}_c \tag{3.1}$$

Also it is assumed that the body force could be computed by taking the integral of a vector field $\boldsymbol{b}(\boldsymbol{r}, t)$ over its volume:

$$\boldsymbol{f}_b = \int_V \boldsymbol{b}(\boldsymbol{r}, t)\rho dV \tag{3.2}$$

where, V is the volume of the body, ρ is the density of the material, **r** is the position vector with respect to the origin in Eulerian coordinates, and t is time.

Similarly the contact force is defined by integrating a vector field $\boldsymbol{t}(\boldsymbol{r}, \boldsymbol{n})$ acting on the body surface.

$$\boldsymbol{f}_c = \int_{\partial R} \boldsymbol{t}(\boldsymbol{r}, \boldsymbol{n}) ds \tag{3.3}$$

where, n is the unit normal and ds is the infinitesimal surface of the material.

The total force on the body causes the body to move with an acceleration **a**, therefore:

$$\boldsymbol{f} = \int_V \boldsymbol{a}\rho dV \tag{3.4}$$

Thus the relationship mentioned earlier for total force will become:

$$\int_V \boldsymbol{a}\rho dV = \int_V \boldsymbol{b}(\boldsymbol{r},t)\rho dV + \int_{\partial R} \boldsymbol{t}(\boldsymbol{r},\boldsymbol{n})ds \tag{3.5}$$

According to Cauchy's fundamental theorem, at the boundary surface of the body:

$$\boldsymbol{t} = \boldsymbol{\sigma}.\boldsymbol{n} \tag{3.6}$$

where, $\boldsymbol{\sigma}$ is the Cauchy stress tensor. By substituting Equation 3.6 into Equation 3.5 and applying the divergence theorem the surface integral becomes as a volume integral:

$$\int_V \boldsymbol{a}\rho dV = \int_V \boldsymbol{b}(\boldsymbol{r},t)\rho dV + \int_V \boldsymbol{\sigma}.\boldsymbol{\nabla} dV \tag{3.7}$$

where, $\boldsymbol{\nabla}$ is the divergence operator. Utilizing the equation above, Cauchy's first law of motion will become:

$$\boldsymbol{a}\rho = \boldsymbol{b}\rho + \boldsymbol{\sigma}.\boldsymbol{\nabla} \tag{3.8}$$

3.3 Thermodynamic formulation

3.3.1 The First Law of Thermodynamics

The first law of thermodynamics is about the conservation of energy in a system. In solid mechanics, the total energy is a summation of mechanical energy and heat energy. The mathematical representation of total energy is illustrated as follows:

$$\dot{E} = P_{input} + Q_{input} \tag{3.9}$$

In the equation above, P_{input} is the energy input due to mechanical work and Q_{input} is the rate of change of heat of system. P_{input} could be defined as the following:

$$P_{input} = \int_V \boldsymbol{b}\rho.\boldsymbol{v} dV + \int_S \boldsymbol{v}.\boldsymbol{\sigma}.\boldsymbol{n} dS \tag{3.10}$$

where, $\boldsymbol{v}$ is the velocity vector. Using divergence theorem, the equation above becomes:

$$P_{input} = \int_V \boldsymbol{b}\rho.\boldsymbol{v}dV + \int_V (\boldsymbol{v}.\boldsymbol{\sigma}).\boldsymbol{\nabla}dV \tag{3.11}$$

Q_{input} is the sum of the heat rate of internal source of the system and the heat flux through the boundary of the system, therefore it could be written as:

$$Q_{input} = \int_V r\,dV - \int_S \boldsymbol{q}.\boldsymbol{n}dS \tag{3.12}$$

Using the divergence theorem, Equation 3.12 becomes:

$$Q_{input} = \int_V r\,dV - \int_V \boldsymbol{q}.\boldsymbol{\nabla}dV \tag{3.13}$$

Considering Equation 3.11 and by working on the right hand side, it becomes:

$$(\boldsymbol{v}.\boldsymbol{\sigma}).\boldsymbol{\nabla} = \boldsymbol{v}.(\boldsymbol{\sigma}.\boldsymbol{\nabla}) + Tr\big((\boldsymbol{v}\boldsymbol{\nabla}).\boldsymbol{\sigma}\big) \tag{3.14}$$

$Tr\big((\boldsymbol{v}\boldsymbol{\nabla}).\boldsymbol{\sigma}\big)$ is the trace operation. It reflects the summation of diagonal components of a tensor. Utilizing the Cauchy's law of motion equation the following is obtained:

$$P_{input} = \int_V \rho\boldsymbol{a}.\boldsymbol{v}dV + \int_V Tr\big((\boldsymbol{v}\boldsymbol{\nabla}).\boldsymbol{\sigma}\big)dV \tag{3.15}$$

$$P_{input} = \int_V \rho\dot{\boldsymbol{v}}.\boldsymbol{v}dV + \int_V Tr\big((\boldsymbol{v}\boldsymbol{\nabla}).\boldsymbol{\sigma}\big)dV \tag{3.16}$$

By substituting the equations above into Equation 3.9, it will be represented as:

$$\dot{E} = \int_V \rho\dot{\boldsymbol{v}}.\boldsymbol{v}dV + \int_V Tr\big((\boldsymbol{v}\boldsymbol{\nabla}).\boldsymbol{\sigma}\big)dV + \int_V r\,dV - \int_V \boldsymbol{q}.\boldsymbol{\nabla}dV \tag{3.17}$$

Also, the total energy of a system could be written as a summation of total kinetic energy and internal energy:

$$E = \int_V \frac{1}{2}\rho(\boldsymbol{v}.\boldsymbol{v})dv + \int_V \rho u dV \tag{3.18}$$

where u is the specific internal energy where the word "specific" means per unit mass. By differentiating the equation above with respect to time, the rate form of total energy becomes as:

$$\dot{E} = \frac{d}{dt}\left(\int_V \frac{1}{2}\rho(\boldsymbol{v}.\boldsymbol{v})dv + \int_V \rho u dV\right) = \int_V \rho \dot{\boldsymbol{v}}.\boldsymbol{v} dV + \int_V \rho \dot{u} dV \tag{3.19}$$

Combining Equations 3.17 and 3.19, the result will be:

$$\rho \dot{u} = Tr\big((\boldsymbol{v}\boldsymbol{\nabla}).\boldsymbol{\sigma}\big) + \rho r - \boldsymbol{q}.\boldsymbol{\nabla} \tag{3.20}$$

By decomposing matrix $\boldsymbol{v}\boldsymbol{\nabla}$ into symmetric and anti-symmetric matrices, the rate of deformation tensor, D, and rate of rotation tensor, W, is obtained as follows:

$$\boldsymbol{D} = \frac{1}{2}(\boldsymbol{v}\boldsymbol{\nabla} + (\boldsymbol{v}\boldsymbol{\nabla})^{\boldsymbol{T}}) \tag{3.21}$$

$$\boldsymbol{W} = \frac{1}{2}(\boldsymbol{v}\boldsymbol{\nabla} - (\boldsymbol{v}\boldsymbol{\nabla})^{\boldsymbol{T}}) \tag{3.22}$$

Since in this project, the deformations induced in concrete due to fatigue loading as well as monotonic loading after cycles of freeze-thaw are significantly small; therefore, the rate of deformation tensor D is assumed to be equal to the rate of strain tensor. As a result, Equation 3.20 will become as follows:

$$\rho \dot{u} = \boldsymbol{\sigma}: \dot{\boldsymbol{\varepsilon}} + \rho r - \boldsymbol{q}.\boldsymbol{\nabla} \tag{3.23}$$

In the equation above ':' represents the tensor contraction operator. One could notice that the rate of change of the internal energy per unit volume comprises three parts. $\boldsymbol{\sigma}: \dot{\boldsymbol{\varepsilon}}$ represents the mechanical work input in the system, ρr incorporates the changes in heat due to internal heat source, and $\boldsymbol{q}.\boldsymbol{\nabla}$ represents the heat flow through the boundary of the system.

3.3.2 The Second Law of Thermodynamics

The first law of thermodynamics stated that the total energy in a system is constant and energy can transform/convert from one form to another without any energy dissipation. However, this is not a fact in reality, and energy could dissipate through different irreversible processes like friction. Therefore, to capture such irreversible processes, the second law of thermodynamics has been used.

The second law of thermodynamics states that the rate of change of entropy in a system must be equal to or greater than the rate at which entropy is added by heat flux through the boundaries of the system and by the external heat source. Therefore, the Clausius-Duhem inequality is represented as follows:

$$\frac{d}{dt}\int_V \rho s dV \geq \int_V \frac{\rho r}{\theta} dV - \int_S \frac{\boldsymbol{q}}{\theta}.\boldsymbol{n} dS \tag{3.24}$$

In the equation above, "s" represents the entropy and "θ" is the absolute temperature. If the inequality above becomes equal then it implies a reversible process. By applying the divergence theorem on the Clausius-Duhem inequality, it changes to:

$$\int_V \rho \dot{s} dV \geq \int_V \frac{\rho r}{\theta} dV - \int_V \frac{\boldsymbol{q}}{\theta} . \boldsymbol{\nabla} dV \tag{3.25}$$

$$\rho \dot{s} \geq \frac{\rho r}{\theta} - \frac{\boldsymbol{q}}{\theta} . \boldsymbol{\nabla} \tag{3.26}$$

By introducing $\dot{\eta}$ representing the rate of internal entropy production, the inequality shown above changes to the form below. This equation could be interpreted as additional entropy produced in a different way than an internal heat source or heat flux through boundaries of the system.

$$\rho \dot{\eta} = \rho \dot{s} - \frac{\rho r}{\theta} + \frac{\boldsymbol{q}}{\theta} . \boldsymbol{\nabla} \geq 0 \tag{3.27}$$

With some mathematical manipulation, the equation above becomes:

$$\rho \dot{\eta} = \rho \dot{s} - \frac{\rho r}{\theta} + \frac{(\boldsymbol{\nabla} . \boldsymbol{q})}{\theta} - \frac{(\boldsymbol{\nabla}\theta) . \boldsymbol{q}}{\theta^2} \geq 0 \tag{3.28}$$

Moreover, by incorporating the rate of change in internal energy of the system and some modifications, the equation above could be re-written in the format below:

$$\dot{\eta} = \dot{s} - \frac{\dot{u}}{\theta} + \frac{\boldsymbol{\sigma} : \dot{\boldsymbol{\varepsilon}}}{\rho\theta} - \frac{(\boldsymbol{\nabla}\theta) . \boldsymbol{q}}{\rho\theta^2} \geq 0 \tag{3.29}$$

3.3.3 Thermodynamic Potentials and Damage Mechanics

In order to obtain thermodynamic potentials, including Gibbs Free Energy (G), Helmholtz Free Energy (A), and Enthalpy (h), Legendre Transformation is used. The relationship between thermodynamic potentials is defined as follows:

$$u - A + g - h = 0 \tag{3.30}$$

Utilizing the Legendre Transformation leads to the following functional forms:

$$A = u(s, \boldsymbol{\nu}_i) - \theta s \tag{3.31}$$
$$h = u(s, \boldsymbol{u}_i) - \boldsymbol{\tau}_i \boldsymbol{\nu}_i \tag{3.32}$$
$$g = h(s, \boldsymbol{\tau}_i) - \theta s \tag{3.33}$$
$$G = -g \tag{3.34}$$

In the equations above, $\boldsymbol{\nu}_i$ is a set of internal parameters used to describe the state of a material. For small deformation, the relationship between Gibbs Free Energy, Helmholtz Free Energy, and internal energy are defined as:

$$A(\boldsymbol{\varepsilon}, \theta) = U(\boldsymbol{\varepsilon}, s) - \theta s \tag{3.35}$$
$$G(\boldsymbol{\sigma}, \theta) = \boldsymbol{\sigma}: \boldsymbol{\varepsilon} - A(b, \theta) \tag{3.36}$$

where $\boldsymbol{\nu}_i$ are interpreted as components of the strain tensor and $\boldsymbol{\tau}_i$ are interpreted as the components of the Cauchy stress tensor. The following equations can be obtained as:

$$u = \boldsymbol{\sigma}: \boldsymbol{\varepsilon} + \theta s - G \tag{3.37}$$
$$\dot{u} = \dot{\boldsymbol{\sigma}}: \boldsymbol{\varepsilon} + \boldsymbol{\sigma}: \dot{\boldsymbol{\varepsilon}} + \dot{\theta} s + \theta \dot{s} - \dot{G} \tag{3.38}$$

By plugging the equations above into Clausius-Duhem inequality, we will have:

$$\dot{G} - \dot{\boldsymbol{\sigma}}: \boldsymbol{\varepsilon} - \dot{\theta} s - \frac{\boldsymbol{q}. \theta \boldsymbol{\nabla}}{\theta} \geq 0 \tag{3.39}$$

The Gibbs free energy could be written as a function of stress, absolute temperature, and damage parameter.

$$\dot{G}(\boldsymbol{\sigma}, \theta, k) = \frac{\partial G}{\partial \boldsymbol{\sigma}}: \dot{\boldsymbol{\sigma}} + \frac{\partial G}{\partial \theta} \dot{\theta} + \frac{\partial G}{\partial k} \dot{k} \tag{3.40}$$

Inserting the above equation into Equation 3.39 results in:

$$\left(\frac{\partial G}{\partial \boldsymbol{\sigma}} - \boldsymbol{\varepsilon}\right): \dot{\boldsymbol{\sigma}} + \left(\frac{\partial G}{\partial \theta} - s\right) \dot{\theta} + \frac{\partial G}{\partial k} \dot{k} - \frac{\boldsymbol{q}. \theta \boldsymbol{\nabla}}{\theta} \geq 0 \tag{3.41}$$

Since the equation above should hold true for any value of $\dot{\boldsymbol{\sigma}}$ and $\dot{\theta}$, the following conclusion could be drawn:

$$\frac{\partial G}{\partial \boldsymbol{\sigma}} - \boldsymbol{\varepsilon} = 0 \tag{3.42}$$
$$\frac{\partial G}{\partial \theta} - s = 0 \tag{3.43}$$
$$\frac{\partial G}{\partial k} \dot{k} - \frac{\boldsymbol{q}. \theta \boldsymbol{\nabla}}{\theta} \geq 0 \tag{3.44}$$

Equation 3.44 is called dissipation inequality and represents the dissipative mechanism. If in a system no damage occurs, then the first term in Equation 3.44, which is a representation of damage rate, will be zero and the second term should be negative in order to satisfy Equation 3.44. This complies with the principle of thermodynamics, which argues that heat travels from high to low temperature. The following results also could be concluded from Equation 3.42 and 3.43:

$$\frac{\partial G}{\partial \boldsymbol{\sigma}} = \varepsilon \tag{3.45}$$

$$\frac{\partial G}{\partial \theta} = s \tag{3.46}$$

Equations above show that by differentiating Gibbs Free Energy with respect to stress and absolute temperature, the results will be strain and entropy, respectively. Also, it could be further assumed that by taking the second derivative of Gibbs Free Energy with respect to stress and absolute temperature, the material compliance C and Specific heat ζ can be obtained, respectively. The mathematical representations of the definitions mentioned above with the definition of thermal expansion tensor **β** are shown in the following equations.

$$\frac{\partial^2 G}{\partial \boldsymbol{\sigma}^2} = \boldsymbol{C}(k) \tag{3.47}$$

$$\frac{\partial^2 G}{\partial \boldsymbol{\sigma} \partial \theta} = \boldsymbol{\beta}(k) \tag{3.48}$$

$$\frac{\partial^2 G}{\partial \theta^2} = \zeta(k) \tag{3.49}$$

In this research work, the effects of temperature on modeling the behavior of concrete under loading have been ignored. The general form of the Gibbs Free Energy could be obtained in the form below as a function of stress, temperature, and damage:

$$G(\boldsymbol{\sigma}, k, \theta) = \frac{1}{2}\boldsymbol{\sigma}:\boldsymbol{C}(k):\boldsymbol{\sigma} + \boldsymbol{\sigma}:\boldsymbol{\varepsilon}^i(k) + \boldsymbol{\sigma}:\boldsymbol{\beta}(k)(\theta - \theta_0) - A^i(k) \tag{3.50}$$

In the equation above, $\boldsymbol{\sigma}$ is the stress tensor, $\boldsymbol{C}(k)$ is compliance tensor, $\boldsymbol{\varepsilon}^i(k)$ is the plastic strain tensor, which represents the irreversible deformation, $\boldsymbol{\beta}(k)$ is the thermal expansion tensor, θ_0 is the reference temperature, and $A^i(k)$ is Helmholtz Free Energy. By assuming that the effects of temperature is negligible in the process of damaging the concrete, the Gibbs Free Energy could be written as the following:

$$G(\boldsymbol{\sigma}, k, \theta) = \frac{1}{2}\boldsymbol{\sigma}:\boldsymbol{C}(k):\boldsymbol{\sigma} + \boldsymbol{\sigma}:\boldsymbol{\varepsilon}^i(k) - A^i(k) \tag{3.51}$$

This is the general form of Gibbs Free Energy used by Yazdani (1993) and Wen et al. (2012) in order to describe the behavior of concrete under biaxial monotonic and cyclic loading.

3.4 Damage Surface and Constitutive Relation

The dissipation inequality, which was a result of second law of thermodynamics, is expressed here again based on Gibbs Free Energy as:

$$\Psi(\boldsymbol{\sigma}, k)\dot{k} \geq 0 \tag{3.52}$$

Where

$$\Psi(\boldsymbol{\sigma}, k) = \frac{\partial G(\boldsymbol{\sigma}, k)}{\partial k} \tag{3.53}$$

Since the damage occurred during the process of loading into the concrete is an irreversible process, no healing can happen in damaged concrete, therefore, it could be assumed that:

$$\dot{k} \geq 0 \tag{3.54}$$

As a result, the following observation could be drawn using the assumption made above and incorporating it into dissipation inequality.

$$if\ \Psi < 0 \quad then \quad \dot{k} = 0 \tag{3.55}$$
$$if\ \Psi \geq 0 \quad then \quad \dot{k} \geq 0 \tag{3.56}$$

Equations 3.55 and 3.56 represent the necessary condition for the onset of damage, but not sufficient. One could say that $\Psi < 0$ is associated with a condition at which material has an elastic behavior. $\Psi < 0$ represents an elastic region, which is surrounded by a damage surface defined by $\Psi = 0$. To provide sufficient condition, the loading-unloading criteria are stated:

$$\Psi = 0\ , \frac{\partial \Psi}{\partial \boldsymbol{\sigma}} : \dot{\boldsymbol{\sigma}} > 0 \quad \rightarrow \quad \dot{k} > 0 \tag{3.57}$$
$$Otherwise \quad \dot{k} = 0$$

To progress further, it is assumed that the deformation can be decomposed into three parts:

$$\boldsymbol{\varepsilon} = \boldsymbol{\varepsilon}^0 + \boldsymbol{\varepsilon}^D + \boldsymbol{\varepsilon}^i \tag{3.58}$$

where $\boldsymbol{\varepsilon}^0$ is the elastic part of the deformation, which occurs before any damage takes place and is associated with the initial or undamaged compliance tensor. $\boldsymbol{\varepsilon}^D$ is the strain that occurs due to damage happening in the material and is called elastic damage. This process represents a reversible deformation associated with the formation of perfect fracture surfaces. The last term in the equation above is $\boldsymbol{\varepsilon}^i$, which represents the inelastic strain and is caused by misfit of crack surfaces.

The following equations represent the concepts of initial compliance tensor, added flexibility, and the relation with the components of the strain tensor.

$$\boldsymbol{C}(k) = \boldsymbol{C}^0 + \boldsymbol{C}^c(k) \tag{3.59}$$

$$\boldsymbol{\varepsilon}^0 = \boldsymbol{C}^0 : \boldsymbol{\sigma}$$

The rate forms of the damage strain tensor and the added flexibility tensor are also shown as: (3.60)

$$\dot{\boldsymbol{\varepsilon}}^D = \dot{\boldsymbol{C}}^c(k) : \boldsymbol{\sigma} \tag{3.61}$$

$\dot{\boldsymbol{C}}^c(k)$ is defined by a fourth order response tensor as the following:

$$\dot{\boldsymbol{C}}^c(k) = \dot{k}\boldsymbol{R}(\boldsymbol{\sigma}) \tag{3.62}$$

The definition of the terms mentioned above was explained in the previous section and will be illustrated again in the following sections. Setting $\Psi(\boldsymbol{\sigma}, k) = 0$, a surface is defined using a damage function, $t(\boldsymbol{\sigma}, k)$.Incorporating the terms defined above into the damage surface equation results in the following equation:

$$\Phi(\sigma, k) = \frac{1}{2}\boldsymbol{\sigma} : \frac{\partial \boldsymbol{C}^c(k)}{\partial k} : \boldsymbol{\sigma} + \frac{\partial \boldsymbol{\varepsilon}^i(k)}{\partial k} : \boldsymbol{\sigma} - \frac{1}{2}t^2(\boldsymbol{\sigma}, k) = 0 \tag{3.63}$$

The thermodynamics principles illustrated in this section will be used in the following sections in order to develop models to predict the changes in the behavior of concrete under fatigue loading as well as freeze-thaw process.

3.5 Strain-Based Damage Model

Thus far, the formulation has been presented in stress space. However, Thapa and Yazdani (2008) developed the formulation in both stress and strain space and proved that both approaches are equivalent.

For strain space, they started with Helmholtz free energy (HFE) for small deformations and isothermal as follows:

$$A(\boldsymbol{\varepsilon}, k) = \frac{1}{2}\boldsymbol{\varepsilon} : \boldsymbol{E}(k) : \boldsymbol{\varepsilon} + A^{\boldsymbol{i}}(k) \tag{3.64}$$

where, $\boldsymbol{\varepsilon}$ represents the strain tensor, k is the scalar damage variable representing dissipation of energy, **E** is the stiffness tensor, and $A^{\boldsymbol{i}}(k)$ is the inelastic component of the HFE associated with the surface energy of microcracks. The dependency of stiffness tensor on damage parameter allows the model to capture the anisotropic nature of induced damage through the components of stiffness tensor.

In their work, Thapa and Yazdani (2008) assumed the following decomposition for the material stiffness tensor as:

$$\boldsymbol{E}(k) = \boldsymbol{E}^0 + \boldsymbol{E}^D(k) \tag{3.65}$$

where, $\boldsymbol{E}^0$ is the stiffness tensor for undamaged material and $\boldsymbol{E}^D$ is the reduced stiffness due to microcracks that occurred during the damage process.

Utilizing the Clausius-Duhem inequality followed by standard thermodynamic arguments, the dissipation inequality becomes:

$$d_s = -\left(\partial A/_{\partial k}\right)\dot{k} \geq 0 \tag{3.66}$$

where, d_s is the dissipating rate.

The substitution of Equations 3.64 and 3.65 into Equation 3.66 results in:

$$d_s = -\left(\frac{1}{2}\right)\boldsymbol{\varepsilon}:\dot{\boldsymbol{E}}^D:\boldsymbol{\varepsilon} - \dot{A}^i \geq 0 \tag{3.67}$$

For a given material under a specified load path, the equation above must give the same result as what is obtained from dissipation inequality from stress space. Considering the constitutive relation as follows:

$$\boldsymbol{\sigma} = \boldsymbol{E}(k):\boldsymbol{\varepsilon} \tag{3.68}$$

and comparing the dissipation inequalities obtained from both stress and strain spaces, the following equation will be obtained:

$$\boldsymbol{\sigma}:\dot{\boldsymbol{C}}^{\boldsymbol{D}}:\boldsymbol{\sigma} = \boldsymbol{\varepsilon}:\dot{\boldsymbol{E}}^{\boldsymbol{D}}:\boldsymbol{\varepsilon} \tag{3.69}$$

which shows the equivalency of both stress and strain approaches.

4 LITERATURE REVIEW

4.1 Modeling of Concrete Under Fatigue Multiaxial Loading

In order to describe the behavior of concrete under multiaxial loading, different approaches have been used. Each approach is used for different scales of damage. There are three types of damage that could be modeled using different approaches:

1. Describing damages corresponding to atomic voids and crystalline defects using material science models at atomic scale.
2. Damages on scales of microcracks and microvoids. Continuum damage mechanics is a good approach to describe such damages.
3. Damages on a scale of macro cracks. Fracture mechanics could be used to model the behavior of material on such a scale. It studies the behavior of the material based on propagation of a discrete crack.

In addition, based on the different parameters, modeling the mechanical behavior of concrete under fatigue loading could be categorized into three groups: fatigue life models, phenomenological residual strength/stiffness models, and progressive damage models.

4.2 Fatigue Model Categories

4.2.1 Fatigue Life Models

The earliest and simplest form of fatigue modeling is fatigue life modeling. In this type of modeling, fatigue damage accumulation during the fatigue process is not considered; therefore, it does not give any information regarding the fatigue damage development into the material and the state of the material in terms of stiffness and deformation at any specific cycles. However, due to its simplicity, it is widely used in industry. Thus, this type of modeling is vastly incorporated into finite element software such as ANSYS and in many engineering standards.

Fatigue life models give information about fatigue life of concrete by representing the strength versus number of cycles of loading as so-called “S-N” curves. “S-N” curves can be presented in the forms of power and logarithm functions.

The power function can be shown in the form of:

$$e^{aS}N = c \tag{4.1}$$

where “a” and “c” are material parameters determined by conducting fatigue experimentation and are functions of material characterization, specimen configuration, and loading methods; “e” is the base of natural logarithm, “S” in the applied stress, and “N” is the fatigue life of corresponding applied load.

The logarithm function can be presented as:

$$S^{a}N = c \tag{4.2}$$

where “a” and “c” are material parameters, “S” is the material strength and “N” is the number of cycles of loading corresponding to the strength of the concrete.

Based on these two forms, various models with different material parameters have been proposed. In addition to loading amplitude and number of cycles of loading, those models have taken other factors affecting the fatigue life of concrete such as stress range, mean stress, and stress ratio (load path) into account.

Aas-Jakobsen and Lenschow (1973) proposed a model that considers the effect of stress range in terms of stress ratio “R” (minimum to maximum fluctuating stress) under compressive loading. They derived the following relationship for S-N curves:

$$\frac{\sigma_{max}}{f_c} = 1 - \beta(1 - R)logN \tag{4.3}$$

where σ_{max} is the maximum applied stress, f_c is the strength of concrete under monotonic loading, “β” is the material parameter representing the slope of the S-N curve when R=0 that was given as 0.064, and “N” is the fatigue life. By conducting their own tests and utilizing other tests results reported in the literature, Tepfers and Kutti (1979) calculated β to be 0.0685.

Although equation 4.3 was a big step toward development of the S-N Curves, it had two shortcomings. First, when R becomes one, $\frac{\sigma_{max}}{f_c}$=1 and σ_{max} becomes a constant. Theoretically, this is incorrect. Rusch (1960) has shown that the sustained strength of concrete is time dependent and the long-time strength can reach approximately 75% of concrete’s monotonic strength. Second, equation 4.3 does not include the rate of loading (frequency) in the model even though this parameter has significant effects on fatigue life of concrete, especially in the case of low-cycle fatigue range. Therefore, Hsu (1981) introduced a new parameter, T, that is the period of the repetitive loads expressed in seconds per cycle and proposed new equations for S-N curves that included T and R and also overcame the shortcomings noted in previous models. By the work of Hsu (1981), the concept of three dimensional S-N-R curves, which was proposed earlier by Aas-Jakobsen and Lenschow (1973), changed to four dimensional S-N-R-T curves.

4.2.2 Phenomenological Models

Phenomenological models, also known as Continuum Damage Mechanics (CDM), models are categorized into to subsections: residual strength models and residual stiffness models.

The residual strength models study the fatigue process by looking at the changes that occur in the strength of the material and assume that the material fails when the residual strength reaches the applied stress.

In this class of modeling, the residual strength is a function of various factors such as amplitude of loading, number of cycles of loading, loading range, loading ratio, and material characterization. Therefore, utilizing the residual strength function, the initial (monotonic) strength of the material decreases by increasing the number of cycles. This process continues to

the point at which the number of cycles of loading reaches the number of failure. At this point, the material fails and will not sustain any additional loads. Wen et al. (2012) and Reberg (2013) have utilized this approach to capture the effects of fatigue loading on woven fabric composites and concrete. Since this research project is based on residual strength models, it will be discussed further in detail at the end of this section.

The residual stiffness models incorporate the damage that occurs during the fatigue process in the elastic properties of material. The nucleation and propagation of microcracks in the material due to cyclic loading is then accompanied by a decrease in the longitudinal modulus of elasticity as well as an increase in the irrecoverable (plastic) strain after unloading (Alliche and Frangois, 1992; Gao and Hsu, 1998).

Under uniaxial fatigue loading, one definition for damage is given as:

$$D = 1 - \frac{E}{E_0} \tag{4.4}$$

where D is the damage variable occurred in the material, E_0 is the initial or undamaged Young's modulus, and E is the modulus of elasticity of the material after the application of fatigue loading. In this approach, D is defined as a damage variable. However, these models do not take the actual directionality of damage into consideration. They use a macro scale mathematical modeling to describe the damage rate as dD/dN. Although describing the fatigue behavior of materials by developing models based on individual cracks might be more accurate, it becomes impossible in the case of concrete due to heterogeneity of the material. In other words, although in metals that crack propagation pattern is based on a single crack propagation in general, in concrete, it is a problem of numerous crack propagation and interaction. Therefore, the macro scale mathematical modeling of damage will be a good approach to simulate the fatigue process in concrete (Wen, 2011).

4.2.3 Progressive Damage Models

In this approach, the damage variables utilized to develop the models are different from what were chosen in the previous approaches. In these models, damage variables such as strain energy release rate, damage area, and crack surface are chosen as study parameters to address the degradation of the materials.

Natarajan et al. (2005) proposed a model based on internal strain energy release rate to describe the fatigue response of fabric-reinforced polymeric composites. They proposed the energy release rate equation as follows:

$$\frac{dU}{dN} = a\left(\frac{\varepsilon_{max}}{\varepsilon_{ult}}\right)^b \tag{4.5}$$

where ε_{max} is the maximum strain, ε_{ult} is the maximum strain at which the material fails under monotonic loading, and "a" and "b" are the material parameters.

Based on the energy release rate equation, Natarajan et al. (2005) proposed the following equation to predict the failure life of the material:

$$N_f = \frac{0.5U_0}{a(\varepsilon_{max}/\varepsilon_{ult})^b} \tag{4.6}$$

where U_0 is the initial internal strain energy. Although this model shows a good correlation with experimental data, for different loading types, different formulas of strain energy will be needed. Among all these three types of modeling, the fatigue life models are simple and easy to use; however, they do not provide all information about changes occurring in material due to fatigue loading. This information includes change of modulus of elasticity and deformation characterization of the material.

The progressive damage models are good to incorporate new damage variables. However, since the propagation of cracks and microcracks forms the major part of fatigue life of concrete, therefore, this approach has to study the fatigue behavior of material by modeling the details of evolution and propagation of every microcrack individually. As a result, due to scattering and widely spread nature of microcracks in concrete, it is obvious that modeling the behavior of every macrocrack becomes a tedious task, if not an impossible one.

The phenomenological models provide information essential to designing purposes while avoiding the formidable task of studying each crack individually. Therefore, the phenomenological models are convenient to be utilized for modeling the fatigue life of concrete and brittle materials and is the chosen approach in this research study to model the behavior of concrete under fatigue loading as well as freeze-thaw process. In the following sections, the fundamental concepts of this approach will be discussed further in detail.

4.3 Continuum Damage Mechanics

Among all these approaches, continuum damage mechanics is the approach utilized in this research study. This approach macroscopically studies the changes in the mechanical behavior of materials such as concrete by introducing an internal variable called the “damage variable” to describe the changes in the material. The models proposed in the framework of continuum damage mechanics are based on the thermodynamics of irreversible processes.

In the following, the basis of continuum damage model proposed by Wen et al. (2012), which predicts the behavior of woven fabric composites under monotonic multiaxial loading as well as fatigue loading, will be explained. In the next sections, two models will be proposed based on Wen’s (2012) model to predict the behavior of concrete under fatigue loading and freeze-thaw processes, and the results will be compared with the data obtained from literature.

4.3.1 Wen Damage Mechanics Model (2012)

Wen (2012) has proposed a damage mechanics model based on Yazdani (1993) model in order to predict the changes in mechanical behavior of woven fabric composite under multiaxial fatigue loading. Wen’s model differs from Yazdani’s (1993) model in several ways, including

response tensors describing the strain, damage function, which is used to describe the onset of damage or the limit surface, and the incorporation of softening function in order to account for fatigue type of loading. Although the Wen (2012) model has been proposed to capture the changes in the mechanical behavior of woven fabric composite under fatigue loading, we will use the same approach to describe changes in the mechanical behavior of concrete under fatigue loading as well as freeze-thaw process in the next sections.

The form of Gibbs Free Energy used in this model is shown below:

$$G(\boldsymbol{\sigma}, k) = \frac{1}{2}\boldsymbol{\sigma}: \boldsymbol{C}(k): \boldsymbol{\sigma} + \boldsymbol{\sigma}: \boldsymbol{\varepsilon}^i(k) - A^i(k) \tag{4.7}$$

Wen et al. (2012) have used the same form of compliance tensor proposed by Ortiz (1985) which is:

$$\boldsymbol{C}(k) = \boldsymbol{C}^0 + \boldsymbol{C}^c(k) \tag{4.8}$$

In the equation above, $\boldsymbol{C}^0$ is the initial compliance tensor of the material before any damage occurred and $\boldsymbol{C}^c(k)$ is added flexibility due to damage occurred during loading. Differentiating the Gibbs Free Energy with respect to stress, the following relationship for strain will be obtained:

$$\boldsymbol{\varepsilon} = \boldsymbol{C}^0: \boldsymbol{\sigma} + \boldsymbol{C}^c(k): \boldsymbol{\sigma} + \boldsymbol{\varepsilon}^i(k) \tag{4.9}$$

The equation above shows that the total strain comprises three terms. The first term is the elastic strain, the second term is the recoverable strain, which is due to elastic damage (microcracking), and the third term is the inelastic (plastic) strain, which is the permanent deformation in the material. Wen et al. (2012) have defined the additional flexibility $\boldsymbol{C}^c(k)$ is composed of two terms. Each term has been defined for one type of damage mode caused by compressive or tensile loading. Microcracking due to compressive loading occurs parallel to the direction of loading while under tensile loading it occurs in perpendicular direction. Therefore, Wen et al. (2012) have introduced the additional flexibility in the form below:

$$\boldsymbol{C}^c = \boldsymbol{C}_I^c + \boldsymbol{C}_{II}^c \tag{4.10}$$

Wen et al. (2012) have defined the response tensors in order to predict the direction at which damage occurs. The rate independent form of damage in compliance tensors have been defined as:

$$\dot{\boldsymbol{C}}_I^c = \dot{k}\boldsymbol{R}_I \qquad \dot{\boldsymbol{C}}_{II}^c = \dot{k}\boldsymbol{R}_{II} \tag{4.11}$$

For irreversible damage, $\dot{k} \geq 0$.

Moreover, Yazdani and Karnawat (1996) have proposed the rate form of inelastic strain as the following:

$$\dot{\boldsymbol{\varepsilon}}^{\iota} = \dot{k}\boldsymbol{M} \tag{4.12}$$

where **M** is a response tensor to describe the plastic strain. The following equation has been introduced in order to represent the scalar function A^i.

$$t^2(k) = 2\frac{\partial A^i}{\partial k} \tag{4.13}$$

By utilizing the Gibbs Free Energy and the equation above, Wen et al. (2012) have calculated the damage surface equation as the following:

$$\Psi(\sigma, k) = \frac{1}{2}\boldsymbol{\sigma}^+ : \boldsymbol{R}_I : \boldsymbol{\sigma}^+ + \frac{1}{2}\boldsymbol{\sigma}^- : \boldsymbol{R}_{II} : \boldsymbol{\sigma}^- + \boldsymbol{\sigma} : \boldsymbol{M} - \frac{1}{2}t^2(\boldsymbol{\sigma}, k) \geq 0 \tag{4.14}$$

$\boldsymbol{\sigma}^+$ and $\boldsymbol{\sigma}^-$ are the positive and negative cones of stress tensor. This equation represents the damage surface and is true when the damage occurs. If no damage occurs in the material, it means that the material is in elastic state and the elastic region is enclosed by the damage surface defined by the aforementioned equation. Two conditions should be met in order for damage to occur in the material. First, the point of stress must fall on the damage surface described by the equation above, and second, the stress increment should point outside the damage surface. These two conditions could be stated as below:

$$\Psi(\boldsymbol{\sigma}, k) = 0 \qquad \frac{\partial \Psi}{\partial \boldsymbol{\sigma}} : \dot{\boldsymbol{\sigma}} > 0 \tag{4.15}$$

Wen et al. (2012) have proposed their model for biaxial tension load path. Therefore, in this case, just the response tensor for tension mode of damage has been proposed in the form of:

$$\boldsymbol{R}_I = \frac{\boldsymbol{\sigma}^+ \otimes \boldsymbol{\sigma}^+}{\boldsymbol{\sigma}^+ : \boldsymbol{\sigma}^+} - \alpha(\boldsymbol{I} - \boldsymbol{i} \otimes \boldsymbol{i}) \tag{4.16}$$

where **I** and **i** are the fourth and second order identity tensors, respectively, and α is the material parameter that could be obtained by utilizing experimental data. The second part, brought in the response tensor, is used in order to predict the changes in Poisson's Ratio once damage accumulates.

The second order response tensor **M** used to describe the inelastic strain is proposed in the form shown below:

$$\boldsymbol{M} = \beta\boldsymbol{\sigma} \tag{4.17}$$

β is also a material parameter which could be obtained experimentally.

Thus far, the response tensors for elastic and inelastic strains have been introduced. Strength of woven fabric composites differs in various directions. In addition, material strength will be reduced by applying cyclic loading. Therefore, Wen et al. (2012) proposed a new damage function that incorporates all these features.

In order to incorporate all these features into the model, Wen et al. (2012) used a bounding surface approach. Bounding surface approach states that a loading point in stress space is enclosed by a surface called strength surface. This surface represents the strength of the material either under monotonic loading or under cyclic loading. By utilizing this approach, Wen et al. (2012) have proposed his model for 2-D stress space under biaxial fatigue loading. In the Wen model, limit surface is a surface at which the material fails under monotonic loading. In other words, limit surface is a special condition at which the number of loading is equal to one. In the case of fatigue loading, by increasing the number of loading, the limit surface collapses towards inside and forms smaller surfaces called residual strength. By continuing the loading, this shrinkage continues to a point at which the material fails. At this point, a surface will be formed which represents the failure surface. Figure 4.1. shows the schematic representation of bounding surface approach utilized by Wen et al. (2012).

Utilizing the formulation presented thus far, and incorporating a softening function in order to capture the strength loss in material due to cyclic loading could form the bounding surfaces under fatigue loading. In the following, the bounding surface approach, the damage function, and the softening function proposed by Wen et al. (2012) will be explained in detail. In the end, the results from the model will be compared with the experimental data by Smith and Pascoe (1989).

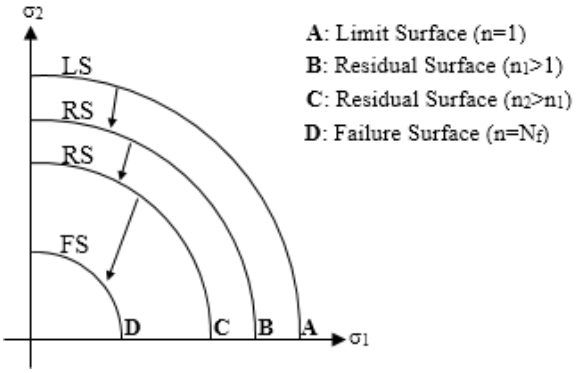

Figure 4.1 Schematic representation of bounding surface approach

The formulation that has been presented so far for fatigue life of woven fabric composites is valid for small deformations and negligible thermal effects. Therefore, these assumptions are valid just in the low frequency fatigue loading.

Wen et al. (2012) proposed the damage function in terms of strength function and shape function in the form of the following:

$$t(\boldsymbol{\sigma}, k) = L(\boldsymbol{\sigma})q(k) \tag{4.18}$$

$q(k)$ is a shape function that has the value of 1 at the failure surface and $L(\boldsymbol{\sigma})$ is a strength function which has the following form:

$$L(\boldsymbol{\sigma}) = \frac{\boldsymbol{\sigma}:\boldsymbol{S}}{tr(\boldsymbol{\sigma})} \tag{4.19}$$

$\boldsymbol{S}$ is a strength tensor, and stress tensor and its trace are used to describe the strength in the proper direction for a given load path.

$$\boldsymbol{S} = \begin{bmatrix} F_{t1} \\ F_{t2} \\ F_{t3} \end{bmatrix} \tag{4.20}$$

Each component of strength tensor represents the strength of the woven fabric composite in a specific direction. These components could be determined by performing monotonic uniaxial tension load tests in the corresponding directions.

By incorporating the response tensors and damage function introduced into the damage surface equation, it becomes:

$$\Psi(\boldsymbol{\sigma}, k) = \boldsymbol{\sigma}:\boldsymbol{\sigma}(1 + \alpha + 2\beta) - \alpha tr^2(\boldsymbol{\sigma}) - \frac{1}{2}\left(\frac{\boldsymbol{\sigma}:\boldsymbol{S}}{tr(\boldsymbol{\sigma})} q(k)\right)^2 = 0 \tag{4.21}$$

To determine the components in strength function, we can introduce uniaxial loading in direction 1. Therefore, the damage surface equation will become:

$$\Psi(\boldsymbol{\sigma}, k) = \begin{bmatrix} \sigma_1 \\ 0 \\ 0 \end{bmatrix} : \begin{bmatrix} \sigma_1 \\ 0 \\ 0 \end{bmatrix} (1 + \alpha + 2\beta) - \alpha tr^2\left(\begin{bmatrix} \sigma_1 \\ 0 \\ 0 \end{bmatrix}\right) - \frac{1}{2}\left(\frac{\begin{bmatrix} \sigma_1 \\ 0 \\ 0 \end{bmatrix} : \begin{bmatrix} F_{t1} \\ F_{t2} \\ F_{t3} \end{bmatrix}}{tr\begin{bmatrix} \sigma_1 \\ 0 \\ 0 \end{bmatrix}} q(k)\right)^2 = 0 \tag{4.22}$$

Then it becomes:

$$(1 + 2\beta)\sigma_1^2 - F_{t1}^2 q^2(k) = 0 \tag{4.23}$$

Under monotonic loading and at the limit surface (damage surface) shape function becomes 1, $q(k) = 1$, and applying stress becomes the tensile strength of the material in that direction, $\sigma_1 = f_{t1}$. Therefore, the first component in the strength tensor becomes:

$$F_{t1} = f_{t1}\sqrt{1 + 2\beta} \tag{4.24}$$

Other components of the strength tensor could be obtained by using the same experimental data but for different directions. Other components of the strength tensor are as follows:

$$F_{t2} = f_{t2}\sqrt{1+2\beta} \qquad F_{t3} = f_{t3}\sqrt{1+2\beta} \tag{4.25}$$

In order to capture the strength reduction in the material due to cyclic loading, Wen et al. (2012) introduced the softening function in the form of power function into the model as the following:

$$F(n) = n^A \tag{4.26}$$

where n is the number of cycles of loading and A is the material parameter. Incorporating the softening function into the damage function, the damage surface equation becomes:

$$\Psi(\boldsymbol{\sigma}, k) = \boldsymbol{\sigma}:\boldsymbol{\sigma}(1+\alpha+2\beta) - \alpha tr^2(\boldsymbol{\sigma}) - \frac{1}{2}\left(\frac{\boldsymbol{\sigma}:\boldsymbol{S}}{tr(\boldsymbol{\sigma})}n^A q(k)\right)^2 = 0 \tag{4.27}$$

By utilizing a fatigue uniaxial tensile loading the material parameter A could be obtained. Therefore, A could be obtained by the following equation:

$$A = \frac{ln\left(\frac{\sigma_1}{f_{t1}}\right)}{\ln(n)} \tag{4.28}$$

Also the material parameter α could be calculated by performing a monotonic equal biaxial tension test in directions 1 and 2. α could be obtained by the following equation:

$$\alpha = 1 - \frac{1}{8}\left(\frac{\sigma_0}{f_{t1}+f_{t2}}\right)^{-2} \tag{4.29}$$

where σ_0 is the applied stress in directions 1 and 2.

In order to show the capabilities of the model to describe the behavior of woven fabric composites under fatigue biaxial loading, experimental data obtained by Smith and Pascoe (1989) are used to compare with the results calculated from the model. Material parameters could be easily calculated based on the equations provided before.

Figures 4.2–4.4 show the S-N curves of a woven fabric composite under various fatigue load paths. As it is shown, the model predicts the reduction in strength of the material due to cyclic loading very well.

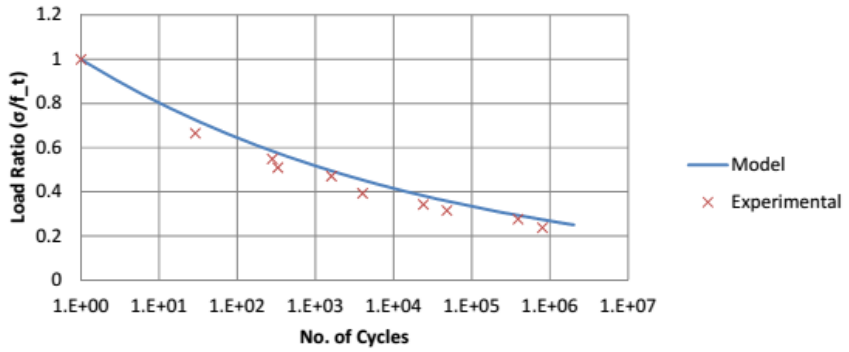

Figure 4.2 S-N curve for woven fabric composite under uniaxial fatigue loading, data by Smith and Pascoe (1989)

Furthermore, Figure 4.5 shows the failure surfaces of the material in the biaxial stress space. The bounding surface concept is noticed in this figure. That is, by applying the fatigue loading, the limit surface collapses and forms smaller surfaces called failure surfaces as shown in the figure. The results obtained by the model show good correlation with the experimental data obtained by Smith and Pascoe (1989).

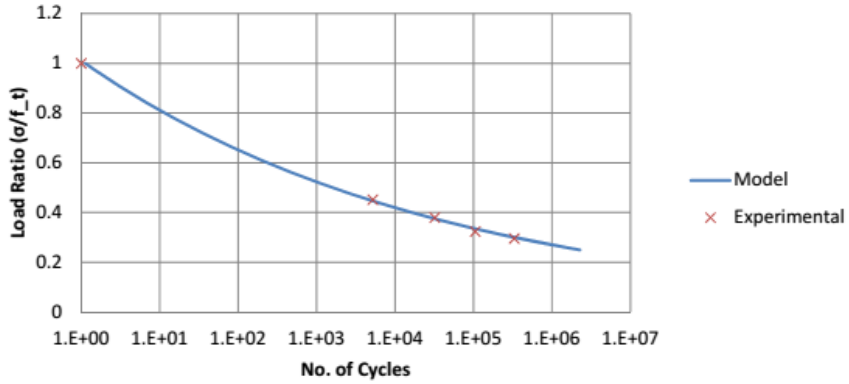

Figure 4.3 S-N curve for woven fabric composite under biaxial fatigue loading with stress ratio of 0.5, data by Smith and Pascoe (1989)

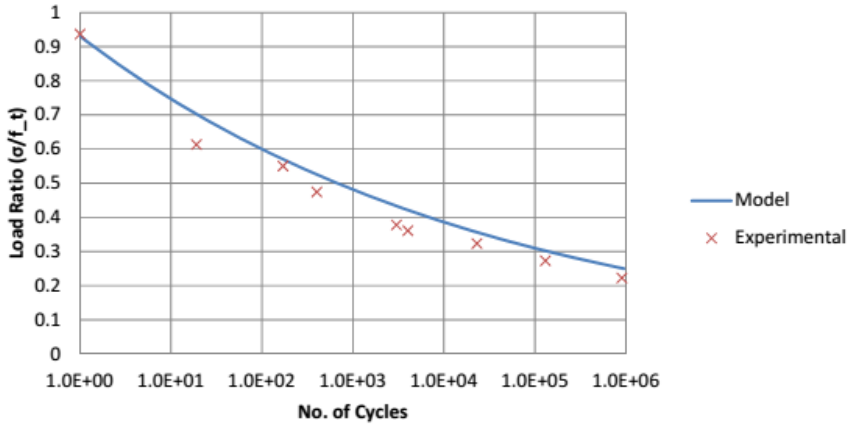

Figure 4.4 S-N curve for woven fabric composite under biaxial fatigue loading with stress ratio of 1, data by Smith and Pascoe (1989)

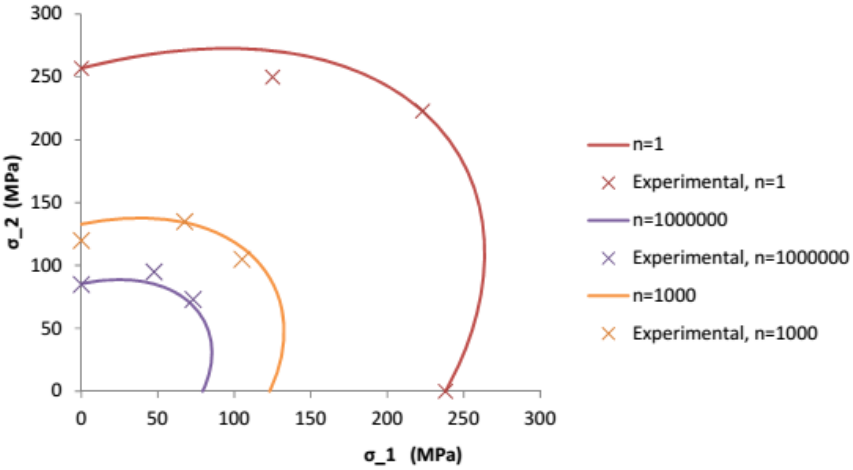

Figure 4.5 Failure surfaces for monotonic and fatigue loading in biaxial stress space, Smith and Pascoe (1989)

5. ANISOTROPIC DAMAGE MODELING OF CONCRETE SUBJECTED TO FREEZE-THAW PROCESS

5.1 Introduction

In recent years, an increased focus has been given to the effects of freeze-thaw cycles on the stiffness and strength properties of concrete as a structural material. Damage caused by frost expansion is a primary concern when designing concrete structures in cold weather regions. It has been shown (Miao et al., 2002; Shang and Song, 2006; Shang and Song, 2008) that the onset of damage within concrete can be accelerated when a freeze-thaw cycle occurs while a structure is subjected to an external loading. This behavior was further investigated by researchers (Hasan et al., 2002; Hasan et al., 2003; Hasan et al., 2008; Shang et al., 2008) showing that the mechanical properties of concrete were adversely affected by the CFT. In all these studies, it was experimentally demonstrated that the strength of concrete decreased substantially with an increase in freeze-thaw cycles. Furthermore, further experimental investigations indicated a more compliant concrete behavior under loading after the application of CFT (Song and Ou, 2008; Duan et al., 2011; Liu and Wang, 2012).

It is generally agreed upon that there are two forms of freeze-thaw damage. The first is caused by hydraulic pressure and is much more prevalent during rapid freezing processes. During this process, water that has been absorbed into the capillary pores of the cement matrix expands once frozen. If the required volume that is needed for expansion is not available, the excess frozen water is transported away by internal pressure. The magnitude of pressure created, as well as the resulting damage, is related to the permeability of the cement matrix, the rate of freezing, the degree of saturation, and the location of the nearest unfilled void within the cement matrix (Pigeon et al., 1985; Detwiler et al., 1989). Localized cracking will take place if the resultant pressure exceeds the tensile strength of the concrete mix. Progressive damage occurs within concrete because with cracking, more volume is available for water to infiltrate and freeze, causing the existing cracks to propagate.

The second form of freeze-thaw damage is termed ice accretion and is more prevalent during long freeze periods and when the rate of freezing is relatively slow. Water in gel pores requires a much lower temperature to freeze, -78° C according to Cordon (1966). This is due to the surface tension forces present in these regions of extremely small radii. For most realistic applications, water in the gel pore zones will remain in a liquid state while it remains in the gel pore. As temperature drops below 0 °C, the water in the gel pores becomes supercooled and has a higher free energy than the ice in the capillaries, which allows the water to move from the gel pores into the capillaries where it is more likely to freeze (Song and Ou, 2008). The overall effect of this process is a reduced volume of the concrete in the form of gel water and an increase in the volume of the capillaries due to expansion of frozen water. Upon thawing, some of the water may return to the gel pores, but the original state of the material will not be obtained as this process is not reversible.

From the experimental data presented by Shang and Song (2006), Shang et al. (2008), and Shang and Song (2008) and the discussion presented by Cordon (1966), it is clear that a meaningful constitutive model needs to be developed to help predict the behavior and performance of

concrete under combined freeze-thaw and applied load conditions. The design life of concrete needs to be taken into consideration so a more efficient, yet safe, design can be obtained.

This section presents a damage mechanics approach to modeling freeze-thaw processes for concrete. Using the bounding surface approach, a limit surface, representing the monotonic strength of concrete, is developed. This surface is allowed to contract as the number of freeze-thaw cycles start to increase. This is similar to the isotropic-softening plasticity used in the modeling of inelastic behavior of materials. The resulting residual strength surface represents the strength of the concrete for various load paths after freeze-thaw processes. Along with proposing softening function during CFT, changes in ultimate strain (strain at which failure occurs) are also addressed. Consequently, stress-stain curves are obtained that describe the behavior of concrete under different proportional load paths.

5.2 General Formulation

The general formulation presented here follows the basic principles of mechanics and internal variable theory of thermodynamics. The intent is to present a model that, although is rigorous in theory, it lends itself well to computational efforts and engineering applications. Guided by the work of Ortiz (1985) and Wen et al. (2012) and for small deformation, the general form of Gibbs Free Energy as a state function is given as:

$$\mathrm{G}(\boldsymbol{\sigma}, \mathrm{k}) = \frac{1}{2}\boldsymbol{\sigma}\colon \mathbf{C}(\mathrm{k})\colon \boldsymbol{\sigma} - \mathrm{A}^{\mathrm{i}}(\mathrm{k}) \tag{5.1}$$

where, **C** is the compliance tensor, **σ** is the stress tensor, k is a scalar damage parameter, and A^i (k) is a scalar function associated with the surface energy of microcracks. The symbol **":"** represents a tensor contraction operation. A class of constitutive model that is considered appropriate for brittle solids such as concrete is given as:

$$\boldsymbol{\varepsilon} = \mathbf{C}(\mathrm{k})\colon \boldsymbol{\sigma} \tag{5.2}$$

where, **ε** represents the strain tensor. The compliance tensor, **C**, is assumed to take an additive decomposition form as:

$$\mathbf{C}(\mathrm{k}) = \mathbf{C}^{0} + \mathbf{C}^{\mathrm{c}}(\mathrm{k}) \tag{5.3}$$

where, $\mathbf{C^0}$ and $\mathbf{C^c}$ are the initial undamaged and the added flexibility tensors, respectively. Because of nonlinearity of constitutive relations caused by damage, the rate form of the flexibility tensor is considered as:

$$\dot{\mathbf{C}}(\mathrm{k}) = \dot{\mathbf{C}}^{\mathrm{c}}(\mathrm{k}) = \dot{\mathrm{k}}\mathbf{R} \tag{5.4}$$

The response tensor, **R**, is used to specify the direction of the induced damage. The Clausius-Duhem inequality can be shown to yield the internal dissipation inequality, which in terms of the Gibbs Free Energy becomes:

$$\frac{\partial G(\boldsymbol{\sigma}, k)}{\partial k}\dot{k} \geq 0 \tag{5.5}$$

It is further assumed that damage is irreversible and that no healing can take place; that is:

$$\dot{k} \geq 0 \tag{5.6}$$

By combining Equations 5.1 through 5.4 and in the absence of any viscosity considered, the general form of the damage surface is given by:

$$\Psi(\boldsymbol{\sigma}, k) = \frac{1}{2}\boldsymbol{\sigma}: \mathbf{R}: \boldsymbol{\sigma} - \frac{1}{2}t^2(\boldsymbol{\sigma}, k) = 0 \tag{5.7}$$

where $t(\boldsymbol{\sigma},k)$ is regarded as the damage function. The condition $\Psi(\boldsymbol{\sigma},k)<0$ represents an elastic domain, and the condition $\Psi(\boldsymbol{\sigma},k)>0$ is not allowed for rate independent processes.

Guided by the experimental work by Smith and Young (1955), the following form for the damage function was proposed by Ortiz (1985) as:

$$t(\boldsymbol{\sigma}, k) = f_c e \frac{\ln(1 + E_0 k)}{(1 + E_0 k)} \tag{5.8}$$

where f_c is the strength of concrete under uniaxial compression, E_0 is the initial modulus of elasticity, and e represents the natural number.

To progress further, a specific form of the response tensor **R** must be stated. It is argued that CFT make no changes on the failure mode of plain concrete (Shang and Song, 2006; Song and Ou, 2008). In this paper, only the compression mode of damage is considered. The damage mode is presented by the response tensor **R** as:

$$\mathbf{R} = \frac{\boldsymbol{\sigma}^- \otimes \boldsymbol{\sigma}^-}{\boldsymbol{\sigma}^-: \boldsymbol{\sigma}^-} + \alpha H(-\lambda)(\mathbf{I} - \mathbf{i} \otimes \mathbf{i}) \tag{5.9}$$

where "$\otimes$" is the tensor product operator, $\boldsymbol{\sigma}^-$ represents the negative cone of the stress tensor, $H(-\lambda)$ is the Heaviside function and λ denotes the maximum eigenvalue of $\boldsymbol{\sigma}^-$. The fourth and second identity tensors are given by **I** and **i**, respectively.

The concept of negative cone of stress tensor is defined in (Ortiz, 1985) and will not be repeated here. In short, $\boldsymbol{\sigma}^-$ is a stress tensor incorporating only the negative eigenvalue of $\boldsymbol{\sigma}$.

5.3 Bounding Surface Approach for Modeling Freeze-Thaw Processes

The concept of bounding surface theory and its application to fatigue type process is a novel one and was recently proposed by Wen et al. (2012). In this approach, the limit surface (LS) is considered to be a special case when the number of freeze-thaw cycles is zero.

To illustrate this further, consider a material element shown in Figure 5.1 and its corresponding limit surface (LS) in biaxial stress space shown in Figure 5.2. The LS corresponds to monotonic strength of the material unaffected by the freeze-thaw damage. As the number of freeze-thaw cycles increases, the strength of the material is expected to decrease, which is represented by the reduction, or inward, collapse of the LS. The collapsing of the LS creates new residual strength surfaces (RS) depending on the number of CFT. At some point, the reduction in strength of the material will result in failure from CFT and under external loading. This is shown in Figure 5.2 as surface "FS" with the corresponding number of freeze-thaw cycles, N_f.

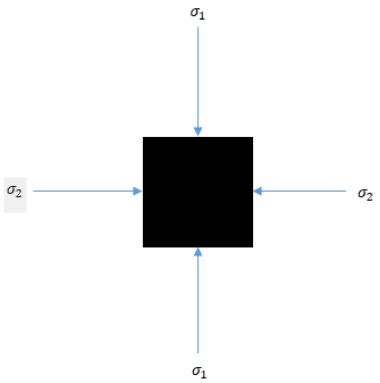

Figure 5.1 Material element with loading directions 1 and 2

To incorporate the effects of the freeze-thaw damage, the damage function t($\boldsymbol{\sigma}$,k) is modified to be given by the product of two functions F(n) and F($\boldsymbol{\sigma}$,k) as:

$$t(\boldsymbol{\sigma}, k(n)) = F_\sigma(n).F(\boldsymbol{\sigma}, k) \tag{5.10}$$

Where, $F_\sigma(n)$ is interpreted as the softening function due to CFT and F($\boldsymbol{\sigma}$,k) is the strength function associated with monotonic loading. The softening function $F_\sigma(n)$ must be formulated in such a way so that the original formulation is retained when CFT is set to zero.

There are two distinct observation that one could make by considering the experimental work of CFT damage (Shang and Song, 2006; Shang et al., 2008). First is that the changes of concrete strength are nearly linear with respect to numbers of freeze-thaw cycles; and second is that the strength reduction is path dependent. The experimental work also indicates that the least damage is to occur under biaxial compression paths with stress ratio of between 0.75 and 1.0 (Shang and Song, 2006). Guided by these studies and observations, the following form of the softening function is proposed as:

$$F_\sigma(n) = \frac{\sigma}{f_c} = 1 - B\left[\frac{\boldsymbol{\sigma}:\boldsymbol{\sigma}}{tr^2(\boldsymbol{\sigma})}\right]^C n \tag{5.11}$$

where, B and C are materials parameters. These parameters can be obtained by utilizing two uniaxial and biaxial compression tests after CFT, respectively.

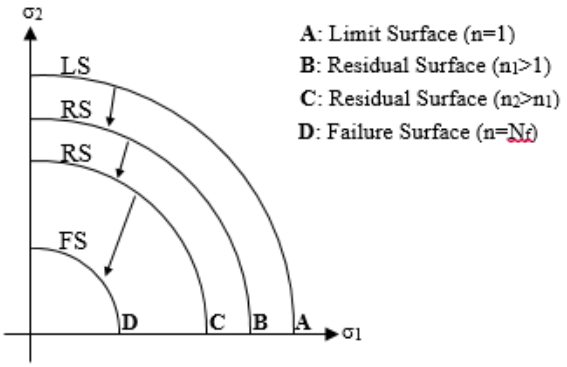

Figure 5.2 Schematic representation of bounding surfaces in biaxial stress space

Thus far, the discussion and formulations have been centered on stress and strength properties of the material. To predict the behavior of concrete under CFT, the deformational characteristics of concrete under CFT also needs to be addressed. In the work presented by Wen et al. (2012), it was assumed that the failure strain, ε_u, remains unchanged under fatigue loading. In the case of concrete under CFT, this assumption will not result in accurate stress-strain behavior since the ultimate strain has been reported to change. A schematic stress-strain behavior of concrete under CFT and consistent with experimental results (Shang and Song, 2006; Shang et al., 2008; Song and Ou, 2008; Duan et al., 2011; Liu and Wang, 2012) is illustrated in Figure 5.3. It shows reduction of strength and subsequently the increase in strain for a given CFT.

Figure 5.4 summarizes the experimental data reported by Shang and Song (2006) on changes in the ultimate strain due to CFT with different stress ratios $\xi=\sigma_1/\sigma_2$. In this figure, a value of $\xi=0$ corresponds to the case of uniaxial compression path. For the equal biaxial load path, ξ becomes equal to 1.0. Figure 5.4 shows that ultimate strains increase with CFT and that the increase is somewhat linear. This increase is attributed to the continuous deformation and propagation of microcracks during the CFT process.

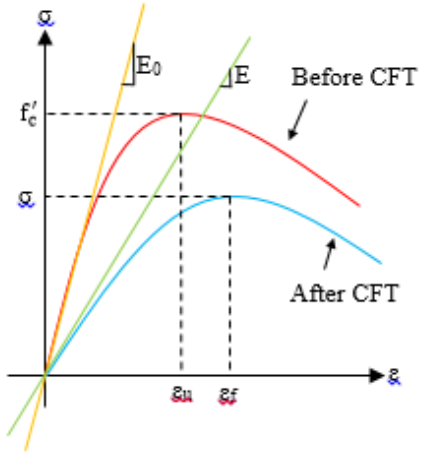

Figure 5.3 Schematic representation of stress-strain curves for concrete before and after applying CFT

Considering the experimental data summarized in Figure 5.4, the following function is postulated as a softening function for the ultimate strain as:

$$F_\varepsilon(n) = \frac{\varepsilon_f}{\varepsilon_u} = 1 + H\left[\frac{\boldsymbol{\sigma}:\boldsymbol{\sigma}}{tr^2(\boldsymbol{\sigma})}\right]^Q n \tag{5.12}$$

where, ε_f is the ultimate strain after CFT, ε_u is the monotonic ultimate strain, and H and Q are material parameters. H and Q are obtained by utilizing uniaxial and biaxial compression tests after a specified number of freeze-thaw cycles, respectively. The motivation for the type of equation shown in Equation 5.12 arises from the observation that it is reasonable to make the softening function linear with "n" as evidenced in Figure 5.4. Also, since the rate of change in strain is path dependent, the path dependency is also captured by the use of invariant shown in the bracket.

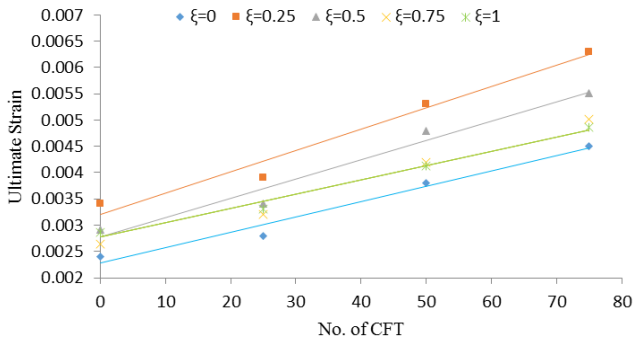

Figure 5.4 Influence of CFT on the principal ε_3 under various stress ratios ($\xi=\sigma_1/\sigma_2$) (Shang and Song, 2006)

5.4 Simulation and Discussion

In this section, the predictive capabilities of the model with respect to freeze-thaw processes is demonstrated in detail for various load paths and number of freeze-thaw cycles. There are a total of five material parameters in the model. Strength parameters are α, B, and C, whereas H and Q are deformational parameters. The strength parameter α can be obtained from a monotonic biaxial strength test. To obtain parameters B and C, uniaxial and biaxial strength tests after a set number of CFT are required. During the same set of CFT tests, the parameters H and Q could also be obtained by taking strain measurements corresponding to the peak stresses.

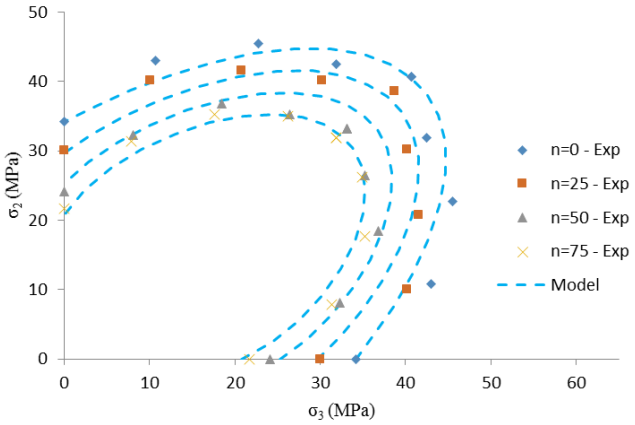

Figure 5.5 Residual strength surfaces for various number of CFT in biaxial compression space (Shang and Song, 2006)

The strength dependency on the number of freeze-thaw cycles, n, is also shown in Figure 5.6 and is compared with the available experimental data. The load path dependency of damage is clearly indicated in this figure where the rate of change of strength reduction is different for different load path groups.

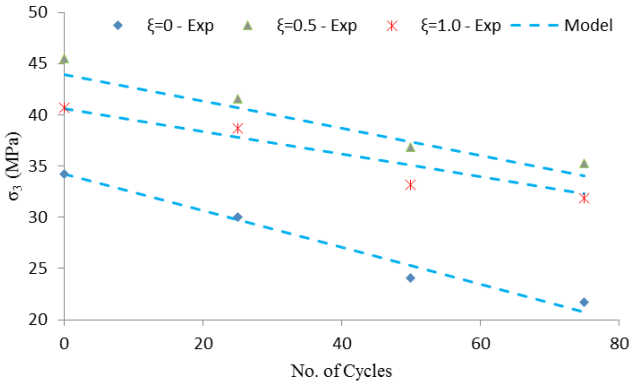

Figure 5.6 Residual strength versus number of CFT in biaxial compression (Shang and Song, 2006)

Based on the experimental data provided by Shang and Song (2006), the following values for parameters are obtained: α=0.645, B=5.223E-03, C=0.944, H=0.0102, and Q=0.359. These values are used to predict material responses for various other load paths. Figure 5.5 represents the biaxial residual strength envelopes where the limit surface and the subsequent residual strength curves are plotted against the experimental data by Shang and Song (2006). The agreement with the experimental data is quite satisfying considering the simplicity of the softening function used (Equation 5.11).

A significant improvement of the proposed model over the existing models is its ability to capture the deformational characteristics of concrete behavior in addition to the stress reduction. These are shown in Figures 5.7, 5.8, and 5.9 where the stress strain responses are predicted for ξ=0, ξ=0.5, and ξ=1.0 and under different numbers of freeze-thaw cycles. Stress reduction as

well as increase in strain are clearly shown in these figures with excellent correlation to experimental data. Also reflected in these figures is the reduction in the stiffness of the material due to freeze-thaw damage. This change in the elastic stiffness is shown in Figure 5.10 for the case of uniaxial compression and compared with the experimental data reported by Liu and Wang (2012).

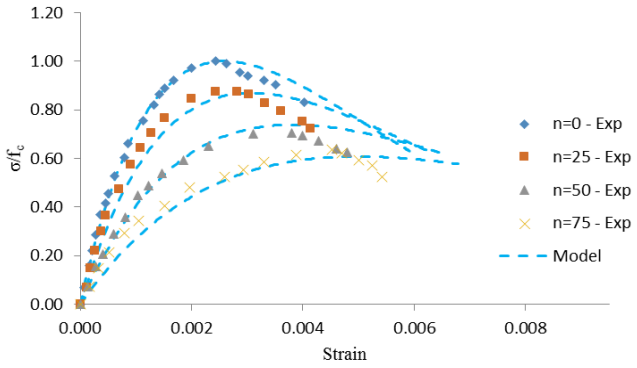

Figure 5.7 Stress-strain curves under uniaxial compression after different CFT (Shang and Song, 2006)

5.5 Conclusion

In this section, the effects of freeze-thaw processes on concrete performance is modeled using a novel bounding surface approach. In this approach, the limit surface that is developed for monotonic loading is allowed to contract as damage takes place with increasing freeze-thaw cycles.

Stress and strain softening functions are postulated guided by the available experimental data. These softening functions are linear with respect to the cycles of freeze-thaw and are structured in such a way to provide load path dependency.

The model was then calibrated with respect to available experimental data and compared with other load paths to show strength reduction, stress-strain curves, and changes of the modulus of elasticity. The model predictions were shown to be satisfactory with respect to salient features of material behavior.

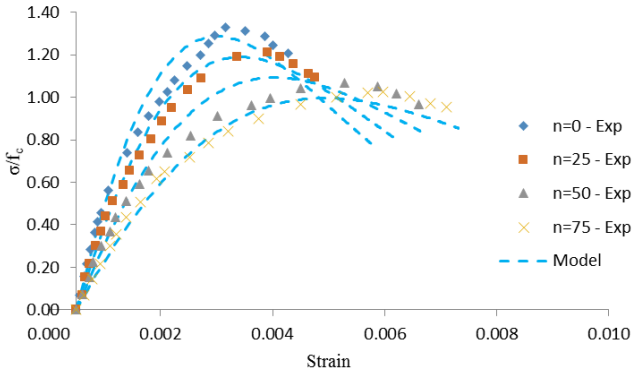

Figure 5.8 Stress-strain under biaxial compression (ξ=0.5) after different CFT (Shang and Song, 2006)

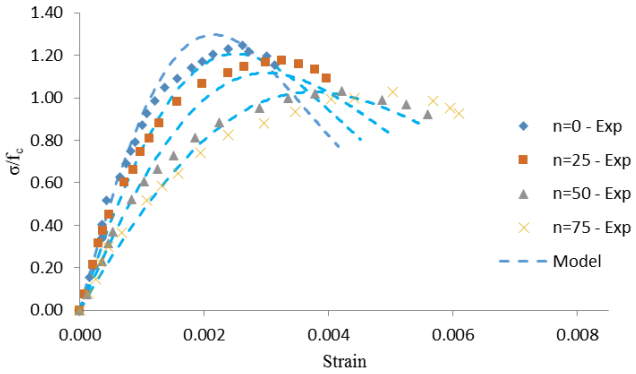

Figure 5.9 Stress-strain under biaxial compression (ξ=0.75) after different CFT (Shang and Song, 2006)

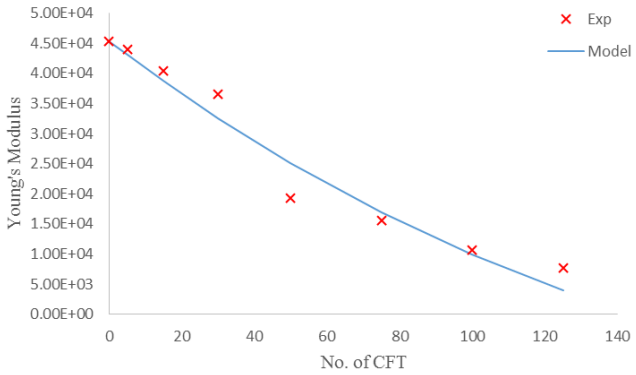

Figure 5.10 Modulus of elasticity versus number of CFT for uniaxial compression (Shang and Song, 2006)

6. ANISOTROPIC DAMAGE MECHANICS MODELING OF CONCRETE UNDER BIAXIAL FATIGUE LOADING

6.1 Introduction

The fatigue behavior of concrete has received considerable attention among researchers in the past two decades. This can be attributed to the increasing use of concrete as a construction material. Concrete has been used in various structures due to its unique features such as high compressive strength, good resistance to aggressive and moist environments compared with other construction materials, and enhancement in strength and deformation capacity under confining stresses. Concrete has been used in dams, bridges, and highway pavements in which cyclic loading is considered as one of the factors affecting its mechanical behavior during its service life. Various research studies have been published on the effects of fatigue loading on the mechanical behavior of concrete in terms of strength, deformation characterization, and modulus of elasticity. Most of these studies were conducted on the uniaxial loading of the material (Awad, 1971; Aas-Jakobsen and Lenschow, 1973; Hsu, 1981; Holmen, 1982; Petkovic et al., 1990; Hordijk and Reinhardt, 1993; Kim and Kim, 1996; Zhang et al., 1996; Paskova and Meyer, 1997; Gao and Hsu, 1998), while only a few studies could be found in the literature on the effects of biaxial stress state loading (Buyukozturk and Tseng, 1984; Nelson et al., 1988; Su and Hsu, 1988; Yin and Hsu, 1995; Lu et al., 2007).

It is generally accepted that concrete under cyclic loading loses its strength gradually with an increase in the number of load cycles regardless of the loading path (uniaxial or biaxial). The strength loss during the fatigue process is due to nucleation and propagation of microcracks. During cyclic loading, these microcracks increase and grow to a stage in which major cracks are formed and reduce the load carrying area tremendously. At that point the strength of the material is decreased substantially and approaches the amplitude of the cyclic loading. This results in sudden rupture. It has been argued that at any given cycle, the fatigue strength of concrete under biaxial compression is greater than that under uniaxial compression (Su and Hsu, 1988; Lu et al., 2007). This is the result of the relative confinement provided in the biaxial loading state. This confinement restricts the nucleation and propagation of microcracks by applying load in two perpendicular directions.

In addition to strength reduction, fatigue loading affects the modulus of elasticity and the deformational capacity of concrete as well. Awad (1971) and Gao and Hsu (1998) have investigated the effects of fatigue loading on the ultimate strain of concrete (strain at which failure occurs) and have concluded that the strain increases under cyclic loading state compared with monotonic state. Awad (1971) has shown that the ultimate and the irreversible plastic strains accumulated after each cycle prior to failure depend on the number of cycles that have been applied. In addition to the maximum stress, it has also been shown that stress range has significant effects on the fatigue life of concrete (Aas-Jakobsen and Lenschow, 1973; Hsu, 1981). By keeping the maximum stress unchanged and decreasing the stress range, the number of cycles to failure will increase. These results have also been investigated and validated by Awad (1971).

According to Gao and Hsu (1998), the fatigue strain of concrete comprises three parts: irreversible strain caused by cyclic creep under the action of average stresses, irreversible strain caused by fatigue cracks, and fatigue strain range. In the same study (Gao and Hsu, 1998), it was reported that the modulus of elasticity of concrete degrades during fatigue process due to damage accumulation, which happens as a result of microcracking.

Realizing the fact that fatigue loading has a significant influence on concrete serviceability and may lead to an abrupt material failure, an accurate and efficient model, which could capture the behavior of concrete, is needed.

In this paper, an approach based on continuum damage mechanics is proposed to model the behavior of concrete under fatigue loading. The general theory of bounding surface approach proposed by Wen et al. (2012) is utilized here in order to capture the strength reduction in concrete due to cyclic loading. In the bounding surface approach, the limit surface is allowed to contract to form smaller surfaces, called residual strength surfaces, as the fatigue loading is applied. A softening function for the loss of strength based on the maximum stress, stress range, and load path is proposed. These features are considered a significant improvement and extension to the work reported by Wen et al. (2012). To capture the effects of fatigue on deformational characterization and material stiffness, two additional softening functions have been proposed to predict the ultimate and plastic strains in the last cycle of loading under any arbitrary fatigue loading. These additional features of the formulation are considered novel, enhancing the predictive capability of the model. At the end, results are compared with experimental data showing a good correlation.

6.2 General Formulation

The general formulation shown in the following is based on the damage mechanics approach and follows the framework of the internal variable theory of thermodynamics. For isothermal and small deformations, the Gibbs Free Energy is obtained as follows (Ortiz, 1985; Yazdani, 1993):

$$G(\boldsymbol{\sigma}, k) = \frac{1}{2}\boldsymbol{\sigma}:\boldsymbol{C}(k):\boldsymbol{\sigma} - A^i(k) \tag{6.1}$$

where **C** is the compliance tensor, **σ** is the stress tensor, k is a scalar damage parameter, and $A^i(k)$ is a scalar function associated with the surface energy of microcracks. The symbol ":" represents a tensor contraction operation. A constitutive relation for concrete like materials is used as:

$$\boldsymbol{\varepsilon} = \boldsymbol{C}(k):\boldsymbol{\sigma} \tag{6.2}$$

where **ε** represents strain tensor. The compliance tensor, **C**, is assumed to take an additive decomposition form as:

$$\boldsymbol{C}(k) = \boldsymbol{C}^0 + \boldsymbol{C}^c(k) \tag{6.3}$$

where $\mathbf{C^0}$ and $\mathbf{C^c}$ are the initial undamaged compliance tensor of the material and the added flexibility tensor associated with the accumulation of damage, respectively. Due to the nonlinearity behavior between stress and strain for brittle materials, the rate form of the flexibility tensor must be considered as:

$$\dot{\boldsymbol{C}}(k) = \dot{\boldsymbol{C}}^c(k) = \dot{k}\boldsymbol{R} \tag{6.4}$$

In Equation 6.4, the response tensor, **R**, determines the direction at which damage occurs. For isothermal and small deformation, the internal dissipation inequality can be represented by Gibbs Free Energy as:

$$\frac{\partial G(\boldsymbol{\sigma}, k)}{\partial k}\dot{k} \geq 0 \tag{6.5}$$

It is also assumed that the damage is an irreversible phenomenon in which, $\dot{k} \geq 0$. By combining Equations 6.1 through 6.5, the general form of the damage surface is given by:

$$\Psi(\boldsymbol{\sigma}, k) = \frac{1}{2}\boldsymbol{\sigma}:\boldsymbol{R}:\boldsymbol{\sigma} - \frac{1}{2}t^2(\boldsymbol{\sigma}, k) = 0 \tag{6.6}$$

where t($\boldsymbol{\sigma}$,k) is called the damage function. The Condition $\Psi(\boldsymbol{\sigma},k)<0$ describes the elastic condition for the material that is enclosed by the damage surface $\Psi(\boldsymbol{\sigma},k)=0$. The condition $\Psi(\boldsymbol{\sigma},k)>0$ is not allowed for rate-independent processes.

Guided by the experimental data (Ortiz, 1985), the following form for the damage function is postulated as:

$$t(\boldsymbol{\sigma}, k) = f_c e\frac{\ln(1 + E_0 k)}{(1 + E_0 k)} \tag{6.7}$$

where f_c is the compressive strength of concrete, E_0 is the initial stiffness, and "e" represents the natural number. In this paper, only the compression mode of damage is considered. Guided by work of Wen et al. (2012) and Saboori et al. (2014), the damage mode is identified by the response tensor **R** given as:

$$\boldsymbol{R} = \frac{\boldsymbol{\sigma}^- \otimes \boldsymbol{\sigma}^-}{\boldsymbol{\sigma}^-:\boldsymbol{\sigma}^-} + \alpha H(-\lambda)(\boldsymbol{I} - \boldsymbol{i} \otimes \boldsymbol{i}) \tag{6.8}$$

where "⊗" is the tensor product operator, $\boldsymbol{\sigma}^-$ represents the negative cone of the stress tensor, $H(-\lambda)$ is defined as the Heaviside function of the maximum eigenvalue of $\boldsymbol{\sigma}^-$, and **I** and **i** are the fourth and second order identity tensors, respectively. The material parameter, α, shown in Equation (6.8), is a strength rated parameter and can be obtained by a biaxial monotonic loading test.

6.3 Bounding Surface Approach

The bounding surface approach for fatigue was proposed by Wen et al. (2012) in order to predict the behavior of woven fabric composites under fatigue loading. This surface is shown schematically in Figure 6.1. In the case of fatigue loading, as cyclic loading is applied, the limit surface is allowed to contract and to form residual strength curves. This reduction in strength is caused by damage and microcracks generated during the fatigue process. As the number of load cycles increases, the strength continues to decrease further, and the residual surfaces also shrink. The reduction in strength continues to a point at which the residual strength becomes equal to the magnitude of loading. At this point, failure surface is formed and the material cannot withstand any additional cycles resulting in failure.

In order to capture the described behavior of concrete under cyclic loading, an evolutionary equation is needed to predict the failure surface. To accomplish this task, the damage function is restructured to be the product of two functions as shown below:

$$t(\boldsymbol{\sigma}, k, n, r) = F(n, r).\, t(\,\boldsymbol{\sigma}, k) \tag{6.9}$$

where F(n,r) is regarded as the strength softening function. The number of cycles of loading to failure is given by "n" and "r" is the stress ratio (ratio of minimum stress to maximum stress). The dependency of the function, t(**σ**,k), on "n" and "r" is supported by the experimental observation described in the previous section.

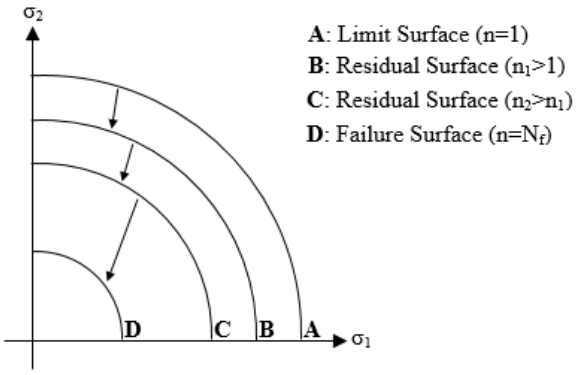

Figure 6.1 Schematic representation of bounding surfaces in biaxial stress space

By considering a fatigue uniaxial compression path and substituting Equation 6.9 into Equation 6.6, the following form is obtained for the softening function:

$$F(n, r) = \frac{\sigma}{f_c} \tag{6.10}$$

where σ is the residual strength of the concrete after a specific number of cyclic loading. Equation 6.10 is a representation of so-called S-n curves. Based on the researches reported in (Aas-Jakobsen and Lenschow, 1973; Hsu, 1981; Qiao and Yang, 2006), amplitude of loading, σ_{max}, stress ratio, r, and finally the load path all contribute to the fatigue life of concrete. While

the fatigue life of concrete is adversely affected by the amplitude of loading, Aas-Jakobsen and Lenschow (1973) reported that increasing stress ratio results in a greater fatigue life at a given stress. Moreover, considering the data provided by Yin and Hsu (1995), it is apparent that the rate of reduction in concrete strength is not the same for different load paths. Guided by these findings, the following softening function is proposed in this paper as:

$$F(n,r) = n^{\left[A(1-r)\left(\frac{tr^2(\boldsymbol{\sigma})}{\boldsymbol{\sigma}:\boldsymbol{\sigma}}\right)^B\right]} \tag{6.11}$$

where n is the number of cyclic loading and "A" and "B" are material parameters. Utilizing this softening function and incorporating it into the Equation 6.6, residual strength surfaces could be obtained under various load paths. The inclusion of the first and second invariants of the stress tensor allows the formulation to model load path dependency observed in fatigue testing.

In Figure 6.2, a schematic representation of stress-strain behavior of concrete, which is consistent with the experimental data (Awad, 1971), is illustrated. The applied stress is signified as σ_{max} and the fatigue failure strain in uniaxial compression is given by ε_{uf}. The figure shows the reduction in strength due to fatigue while the failure strain increases under cyclic loading compared to monotonic loading state.

To fully describe the stress-strain behavior of concrete under fatigue loading, four factors, including reduction in strength, increase in ultimate strain, plastic strain after each cycle, and reduction in modulus of elasticity, need to be addressed. The reduction in strength has already been addressed by the strength softening function (Equation 6.11). For deformation, as was discussed earlier, concrete under fatigue loading fails at an ultimate strain greater than the one under monotonic loading state. Awad (1971) reported that by increasing the stress ratio, both ultimate and plastic strain increases and therefore results in a more flexible concrete. Awad (1971) also showed that amplitude of loading adversely affects both ultimate and residual strains. In order to capture such effects on the mechanical characteristics of concrete, two strain softening functions are presented as follows:

$$F_\varepsilon^t = \frac{\varepsilon_u^f}{\varepsilon_u} = n^{\beta(1+r)} \tag{6.12}$$

$$F_\varepsilon^p = \frac{\varepsilon_f^p}{\varepsilon_u} = n^{\gamma(1+r)} \tag{6.13}$$

where F_ε^t is regarded as the ultimate strain softening function, F_ε^p is residual strain softening function, ε_u^f is the ultimate strain under cyclic loading, ε_u is the ultimate strain under monotonic loading, and ε_f^p is the residual strain under fatigue loading prior to last cycle. The number of cycles of loading to failure is given by "n." The dependency of ultimate and residual strain under fatigue loading reported by Awad (1971) on loading amplitude as well as loading range are addressed by incorporating n and r into Equations 6.12 and 6.13. Utilizing these softening functions, stress-strain curves could be obtained under various load paths. The new proposed model presented by Equations 6.9 and 6.11 for the strength reduction, Equations 6.12 and 6.13 for deformation characterization, and the inclusion of the stress ratio, r, are all new and

considered as significant enhancement of the model compared with the paper by Wen et al. (2012).

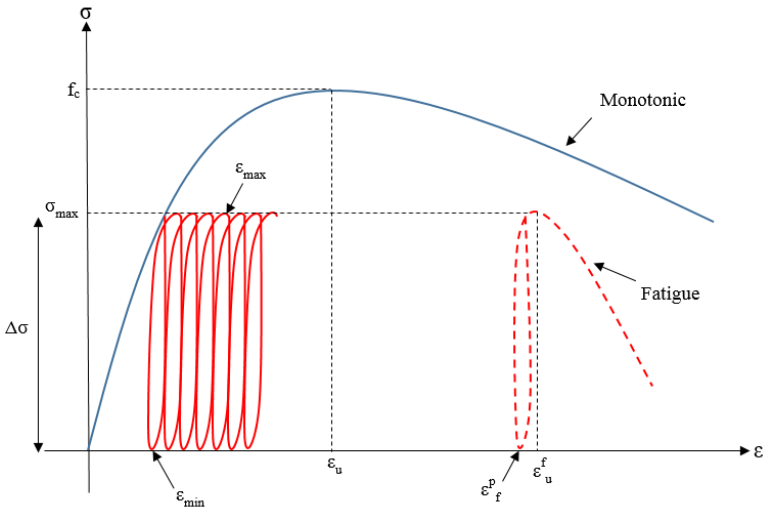

Figure 6.2 Schematic representation of stress-strain of concrete under monotonic and cyclic loading

6.4. Numerical Example

In this section, results predicted by the model are compared with the experimental data obtained from literature. Material parameters α, A, B, β, and γ are calculated based on the experimental data presented.

Figure 6.3 shows the prediction results of residual strength surfaces in biaxial stress space against experimental data work of Nelson et al. (1988). The damage surfaces show a good correlation for monotonic loading when n=1 as well as for fatigue loading when n=10, 100, and 1000 with experimental data. For Figure 6.3, following material parameters are used: α=0.587, A=-0.0445, and B=1.521.

Figures 6.4, 6.5, and 6.6 show the strength versus number of loading cycles for concrete under cyclic uniaxial and biaxial paths with stress ratios of 0.5 and 1.0. These figures show that the strength of concrete materials would decrease with an increase in the number of cycles, n. The rate of strength reduction for these three figures are different, meaning that the strength loss is also dependent on the load path. This is consistent with the experimental data and is captured by the proposed model. For Figures 6.4, 6.5, and 6.6, the following material parameters are used: α=0.745, A=-0.0431, and B=0.552.

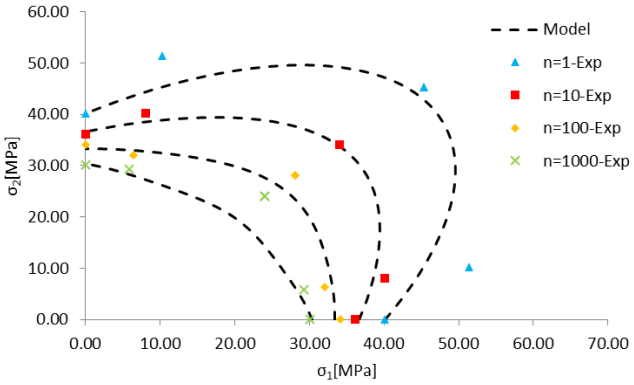

Figure 6.3 Residual strength surfaces for various number of cyclic loading, experimental data by Nelson et al. (1988)

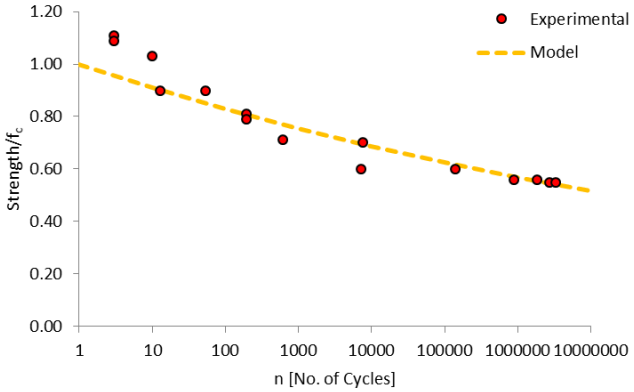

Figure 6.4 S-n curve for concrete under uniaxial cyclic loading, experimental data by Yin and Hsu (1995)

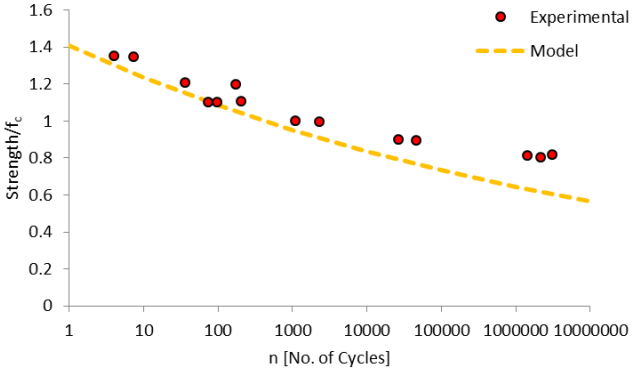

Figure 6.5 S-n curve for concrete under biaxial cyclic loading with stress ratio 0.5, experimental data by Yin and Hsu (1995)

Figure 6.7 illustrates the comparison between the experimental data provided by Awad (1971) and S-n curves obtained by the model for three uniaxial fatigue loading with different stress ratios. As shown, this model captures the effect of stress range on fatigue life of concrete. It can be seen that for any constant stress amplitude, the model predicts a greater fatigue life for a stress

range of 0.65-0.68 than a stress range of 0.41-0.47 and 0, which is consistent with the experimental data in the literature. For the following figures, the material parameters used are: α=0.94, A=-0.0263, β=0.0787, and γ=0.1241.

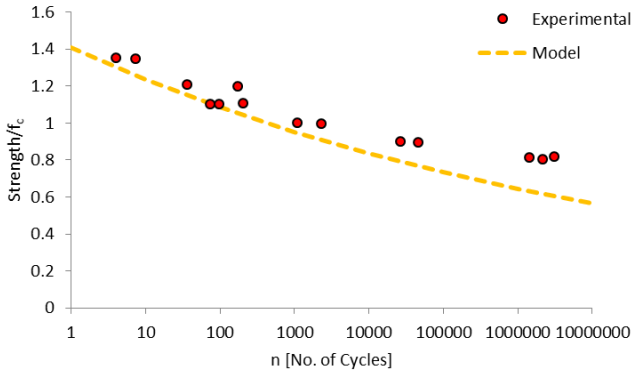

Figure 6.6 S-n curve for concrete under biaxial cyclic loading with stress ratio 1.0, experimental data by Yin and Hsu (1995)

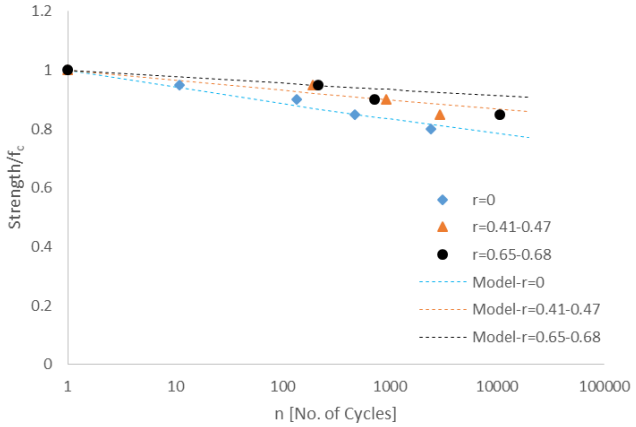

Figure 6.7 S-n curves for concrete under uniaxial loading with various stress ranges, experimental data by Awad (1971)

Figures 6.8 and 6.9 represent the capability of the model in predicting the ultimate strain and residual strain of concrete under uniaxial fatigue loading after different cycles of loading. The model predicts a higher range of ultimate and residual strain for fatigue loading with lower amplitude. This is in conformity with the discussion presented earlier and implies that concrete becomes more flexible under fatigue loading with lower amplitude. Also, Figure 6.9 shows the increase in residual strain by increasing the stress range. That is, for a given "n," the residual strain increases with increasing stress range.

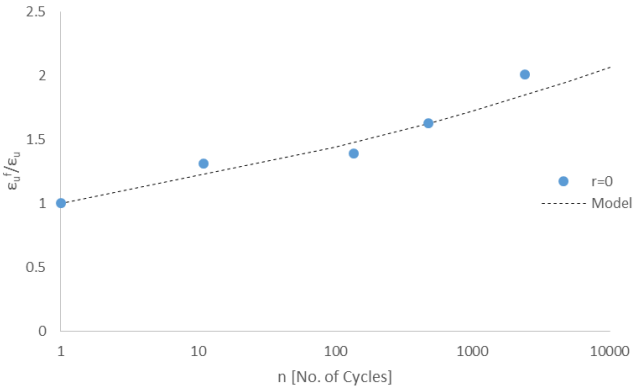

Figure 6.8 Ultimate strain versus number of cycles for concrete under uniaxial cyclic loading, experimental data by Awad (1971)

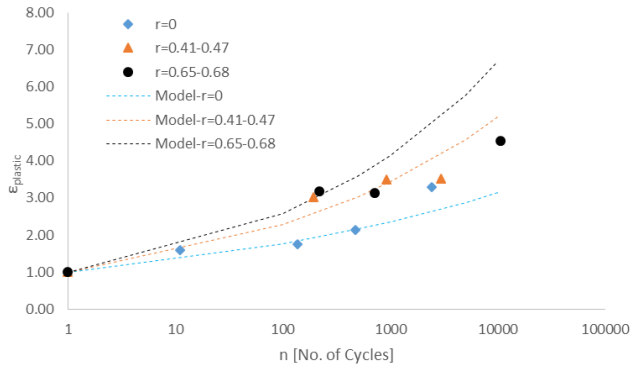

Figure 6.9 Plastic strain versus loading cycles under uniaxial cyclic loading with various stress ranges, experimental data by Awad (1971)

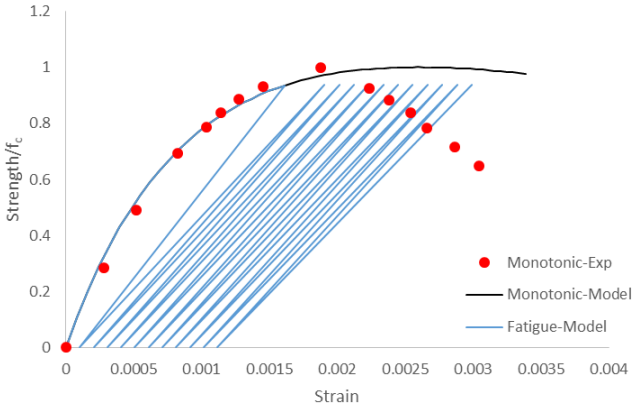

Figure 6.10 Stress-strain curves under cyclic (σmax/fc=0.95) and monotonic uniaxial loading, experimental data by Awad (1971)

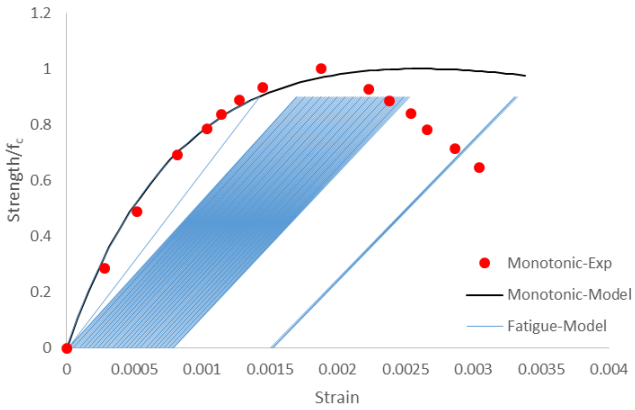

Figure 6.11 Stress-strain curves under cyclic (σ_{max}/fc=0.9) and monotonic uniaxial loading, experimental data by Awad (1971)

Figures 6.10 and 6.11 show the stress-strain curves of concrete under uniaxial monotonic and fatigue loading with amplitudes of $0.95f_c$ and $0.9f_c$. The reduction in strength and longitudinal modulus and increase in ultimate strain are predicted by the model. It can also be noticed that the ultimate and residual strain predicted by the model for fatigue loading with $0.9f_c$ amplitude is greater than the ones for $0.95f_c$ that follows the arguments discussed earlier in the paper. Not all of the cycles to failure are shown in Figure 6.11 for clarity.

6.5 Conclusion

An anisotropic model is utilized to predict the strength behavior of concrete under biaxial compressive fatigue loading. Under cyclic fatigue loading, the limit surface is allowed to contract and form new surfaces identified as residual strength surface. This is accomplished by proposing a softening function that is based on amplitude, stress ratio, and load path. By including these parameters, the effects of strange range and the load paths on the fatigue life of concrete are studied and predicted. Furthermore, to capture the effects of fatigue loading on stress-strain behavior of concrete, two additional strain softening functions are proposed for changes in ultimate and residual (plastic) strains. The influencing factors on ultimate and plastic strains such as amplitude, load path, and load range are incorporated into the proposed softening functions. At the end, the results obtained from the model are compared with the experimental data in the literature showing a good comparison.

7. CONCLUSION AND FUTURE WORK

7.1 Conclusion

Fatigue failure can be named as one of the major failures that occurs in concrete structures such as bridges and pavements. Also, in cold regions like North Dakota where temperature reaches to the level of freezing, the freeze-thaw process can be implied as a destructive process in concrete that induces significant changes in mechanical properties of concrete and its serviceability. However, in both phenomena, not many reliable tests exist to to propose a comprehensive model that takes all the effective factors into consideration. In the case of fatigue loading, although many fatigue tests have been performed, a small portion of those are dedicated to multi axial loading. This could be attributed to the difficulties that exist in such tests. Also, such shortcomings exist in the case of freeze-thaw process as well. In the many freeze-thaw tests that can be found in the literature, the effects of effective factors such as temperature range, frequency of temperature fluctuation, and the duration of the process are not studied even though they have considerable effects on concrete properties.

To model these two processes, in this research, the approach is founded on the first principle of mechanics and thermodynamics. Continuum damage mechanics is also utilized to describe the behavior of concrete under such processes since it is a suitable approach for the crack size smaller than the size of the volume element of a specific material. For brittle and quasi-brittle material like concrete, the main part of fatigue life deals with the first and second stage of the fatigue process, which contains small distributed microcracks. Also, based on the literature, the freeze-thaw process does not change the damage process into the concrete; therefore, this approach is still valid.

To capture induced damage that occurred in the concrete, a response tensor **R** is used. Since the behavior of concrete under compressive loading is studied, the second form of damage is considered. In the case of compressive loading, damage only occurs in the perpendicular direction to the loading direction. Also, concrete strength enhances under biaxial loadings and the damage occurs in the loading direction as well as the non-loading direction.

In order to capture the strength loss in concrete due to fatigue loading and freeze-thaw process, bounding surface approach is used. In this approach, limit surface represents the strength of the material. In the case of fatigue loading, limit surface is a condition at which the number of cyclic loading is equal to one. Applying cyclic loading results in degradation in the material in the form of well-spread microcracks and consequently loss of strength, which ultimately collapses the limit surface and forms new surfaces called residual strength. In order to capture such a behavior, a specific form of the softening function was obtained based on S-N curves available in the literature. Also, due to microcracks that occurred during the cyclic loading, concrete becomes more compliant that, as a result, its failure strain increases compared with failure strain under monotonic loading. Therefore, another softening function for ultimate strain is proposed to capture such a behavior.

In the case of the freeze-thaw process, the limit surface is defined as a condition at which the number of applied freeze-thaw cycles is zero. By applying freeze-thaw cycles to concrete, the limit surface collapses and forms new surfaces called residual strength. Since the mechanism of

generating cracks and damage into concrete in the freeze-thaw process is similar to what occurs under fatigue loading, the same approach is utilized to describe such a process. The difference between the freeze-thaw model and fatigue model in this study is the formulation of their softening functions.

Finally, the models' predictions are compared with the experimental data available in the literature. The results show a good correlation between experimental data and what were obtained from the models. Therefore, it shows that the models are capable of capturing the changes in the mechanical properties of concrete due to both processes well.

7.2 Future Work

Although the models proposed in this research have shown a good correlation with the experimental data, there are still some aspects in the models that can be improved.
In this research, fatigue loading was assumed to be low frequency. Therefore, the thermal effects were neglected in the formulation. It is known that frequency has significant effects on fatigue behavior of concrete, and although the assumption of low frequency loading is still valid in many engineering conditions, there are some high frequency loading conditions that the effects of frequency and the heat generated during the process of loading cannot be ignored. Consequently, incorporating the frequency parameters into the model could improve the accuracy of the results.

In the case of freeze-thaw process, due to lack of experimental data on the effects of different factors such as temperature range, frequency of temperature fluctuation, and duration of the process on mechanical properties of concrete, their effects were not considered in the modeling formulation. Therefore, to improve the model, new experiments can be done to measure the effects of these factors quantitatively and then modify the model accordingly.

REFERENCES

Aas-Jakobsen, K., Lenschow, R. "Behavior of reinforced columns subjected to fatigue loading." *ACI Journal Proceedings*, 1973, ACI.

Ahmed, T., Burley, E., Rigden, S. "The effect of alkali—silica reaction on the fatigue behaviour of plain concrete tested in compression, indirect tension and flexure." *Magazine of Concrete Research*, v. 51, n. 6, p. 375-390, 1999. ISSN 1751-763X.

Alliche, A., Frangois, D. "Damage of concrete in fatigue." *Journal of Engineering Mechanics*, v. 118, n. 11, p. 2176-2190, 1992. ISSN 0733-9399.

Antrim, J. D. C., Mclaughlin, J. F. "Fatigue study of air-entrained concrete." *ACI Journal Proceedings*, 1959, ACI.

Ashby, M. F., Amp. "The failure of brittle solids containing small cracks under compressive stress states." *Acta Metallurgica*, v. 34, n. 3, p. 497-510, 1986. ISSN 0001-6160.

Assimacopoulos, B. M., Warner, R. F., Ekberg, C. E. "High speed fatigue tests on small specimens of plain concrete." *Journal of Prestressed Concrete Institute*, v. 4, n. 2, p. 53-70, 1959.

Awad, M. E. "Strength and deformation characteristics of plain concrete subjected to high repeated and sustained loads." University of Illinois Engineering Experiment Station. College of Engineering. University of Illinois at Urbana-Champaign. 1971

Buyukozturk, O., Tseng, T.-M. "Concrete in biaxial cyclic compression." *Journal of Structural Engineering*, v. 110, n. 3, p. 461-476, 1984. ISSN 0733-9445.

Coleman, B. D., Gurtin, M. E. "Thermodynamics with internal state variables." *The Journal of Chemical Physics*, v. 47, n. 2, p. 597-613, 1967. ISSN 0021-9606.

Cordon, W. A. Freezing and thawing of concrete-mechanisms and control. 1966.

Detwiler, R. J., Dalgleish, B. J., Brady, R. "Assessing the durability of concrete in freezing and thawing." *ACI Materials Journal*, v. 86, n. 1, 1989. ISSN 0889-325X.

Dhir, R., Sangha, R. "Development and propagation of microcracks in plain concrete." *Matériaux et Construction*, v. 7, n. 1, p. 17-23, 1974. ISSN 0025-5432.

Duan, A., Jin, W., Qian, J. "Effect of freeze–thaw cycles on the stress–strain curves of unconfined and confined concrete." *Materials and Structures*, v. 44, n. 7, p. 1309-1324, 2011. ISSN 1359-5997.

Evans, R. H., Marathe, M. S. "Microcracking and stress-strain curves for concrete in tension. Materials and Structures." *Research and Testing*, RILEM, v. 1, p. 61, 1968.

Gao, L., Hsu, C.-T. T. "Fatigue of concrete under uniaxial compression cyclic loading." *ACI Materials Journal*, v. 95, n. 5, 1998. ISSN 0889-325X.

Gopalaratnam, V. S., Shah, S. P. "Softening response of plain concrete in direct tension." *ACI Journal Proceedings*, v. 82, n. 3, p. 310-323, 1985.

Hasan, M. et al. "Tensile stress-crack width model for plain concrete damaged by freezing and thawing action." Proc JCI, v. 24, n. 2, p. 109-114, 2002.

_____. "Stress-strain model of concrete damaged by freezing and thawing cycles." *Journal of Advanced Concrete Technology*, v. 2, n. 1, p. 89-99, 2004. ISSN 1346-8014.

Hasan, M., Okuyama, H., Ueda, T. "The damage mechanism and strain induced in frost cycles of concrete." Proceedings of Japan Concrete Institute. Tokyo: JCI, v. 25, n. 1, p. 401-406, 2003.

Hasan, M., Ueda, T., Sato, Y. "Stress-strain relationship of frost-damaged concrete subjected to fatigue loading." *Journal of Materials in Civil Engineering*, v. 20, n. 1, p. 37-45, 2008. ISSN 0899-1561.

Holmen, J. O. "Fatigue of concrete by constant and variable amplitude loading." *ACI Special Publication*, v. 75, 1982.

Hordijk, D., Reinhardt, H. "Numerical and experimental investigation into the fatigue behavior of plain concrete." *Experimental Mechanics*, v. 33, n. 4, p. 278-285, 1993. ISSN 0014-4851.

Horii, H., Nemat-Nasser, S. "Brittle failure in compression: splitting, faulting and brittle-ductile transition." Philosophical Transactions for the Royal Society of London. Series A, Mathematical and Physical Sciences, p. 337-374, 1986. ISSN 0080-4614.

Hsu, T. T. Fatigue of plain concrete. ACI Journal Proceedings, 1981, ACI.

Karnawat, S. R. "Continuum Representations of Brittle Solids with Application to Concrete." 1997. 193 (Doctor of Philosophy). Civil Engineering and Construction, North Dakota State University, Fargo, North Dakota.

Karsan, I. D., Jirsa, J. O. "Behavior of concrete under compressive loadings." *Journal of the Structural Division*, 1969.

Kestin, J., Rice, J. R. "Paradoxes in the application of thermodynamics to strained solids." Division of Engineering, Brown University, 1969.

Kim, J.-K., Kim, Y.-Y. "Experimental study of the fatigue behavior of high strength concrete." *Cement and Concrete Research*, v. 26, n. 10, p. 1513-1523, 1996. ISSN 0008-8846.

Klcriber, F. W. "The Effects of Air Content, Water-Cement Ratio, and Aggregate Type on the Flexural Fatigue Strength of Plain Concrete." *ACI Special Publication*, v. 75, 1982.

Krajcinovic, D. "Mechanics of solids with a progressively deteriorating structure." In: (Ed.). Application of Fracture Mechanics to Cementitious Composites: Springer, 1985. p.453-479. ISBN 9401087644.

Krajcinovic, D., Fonseka, G. "The continuous damage theory of brittle materials, part 1: general theory." *Journal of Applied Mechanics*, v. 48, n. 4, p. 809-815, 1981. ISSN 0021-8936.

Kupfer, H., Hilsdorf, H. K., Rusch, H. "Behavior of concrete under biaxial stresses." ACI Journal proceedings, 1969, ACI.

Lee, S.-K., Song, Y.-C., Han, S.-H. "Biaxial behavior of plain concrete of nuclear containment building." *Nuclear Engineering And Design*, v. 227, n. 2, p. 143-153, 2004. ISSN 0029-5493.

Liu, M.-H., Wang, Y.-F. "Damage Constitutive Model of Fly Ash Concrete under Freeze-Thaw Cycles." *Journal of Materials in Civil Engineering*, v. 24, n. 9, p. 1165-1174, 2012. ISSN 0899-1561.

Lu, P., Li, Q., Song, Y. "Behavior of concrete under nonproportional biaxial fatigue stresses with one constant." *ACI Materials Journal*, v. 104, n. 1, 2007. ISSN 0889-325X.

LUBLINER, J. "On the thermodynamic foundations of non-linear solid mechanics." *International Journal of Non-Linear Mechanics*, v. 7, n. 3, p. 237-254, 1972. ISSN 0020-7462.

Mehta, P. K., Monteiro, P. J. "Concrete: microstructure, properties, and materials." McGraw-Hill New York, 2006.

Miao, C. et al. "Effect of sulfate solution on the frost resistance of concrete with and without steel fiber reinforcement." *Cement and Concrete Research*, v. 32, n. 1, p. 31-34, 2002. ISSN 0008-8846.

Miner, M. A. "Cumulative damage in fatigue." *Journal of Applied Mechanics*, v. 12, n. 3, p. 159-164, 1945.

Natarajan, V., Gangarao, H. V., Shekar, V. "Fatigue response of fabric-reinforced polymeric composites." *Journal of Composite Materials*, v. 39, n. 17, p. 1541-1559, 2005. ISSN 0021-9983.

Nelson, E. L., Carrasquillo, R. L., Fowler, D. W. "Behavior and failure of high-strength concrete subjected to biaxial-cyclic compression loading." *ACI Materials Journal*, v. 85, n. 4, 1988. ISSN 0889-325X.

Ortiz, M. "A constitutive theory for the inelastic behavior of concrete." *Mechanics of Materials*, v. 4, n. 1, p. 67-93, 1985. ISSN 0167-6636.

Paskova, T., Meyer, C. "Low-cycle fatigue of plain and fiber-reinforced concrete." *ACI Materials Journal*, v. 94, n. 4, 1997. ISSN 0889-325X.

Petkovic, G. et al. Fatigue of high-strength concrete. *ACI Special Publication*, v. 121, 1990.

Pigeon, M., Prevost, J., Simard, J.-M. "Freeze-thaw durability versus freezing rate." *Journal of the American Concrete Institute*, v. 82, n. 5, p. 684-692, 1985.

Pijaudier-Cabot, G., Bazant, Z. P. "Nonlocal damage theory." *Journal of Engineering Mechanics*, v. 113, n. 10, p. 1512-1533, 1987. ISSN 0733-9399.

Qiao, P., Yang, M. "Fatigue life prediction of pultruded E-glass/polyurethane composites." *Journal of Composite Materials*, v. 40, n. 9, p. 815-837, 2006. ISSN 0021-9983.

Raithby, K., Galloway, J. "Effects of Moisture Condition Age, and Rate of Loading on Fatigue of Plain Concrete." *ACI Special Publication*, v. 41, 1974.

Reberg, A. S. "An anisotropic damage mechanics model for concrete with applications for fatigue loading and freeze-thaw effects." 2013. North Dakota State University.

Reinhardt, H. W., Cornelissen, H. A. W., Hordijk, D. A. "Tensile tests and failure analysis of concrete." *Journal of Structural Engineering*, v. 112, n. 11, p. 2462-2477, 1986.

Rusch, H. "Researches toward a general flexural theory for structural concrete." ACI Journal Proceedings, 1960, ACI.

Saboori, A. et al. "Anisotropic damage modeling of concrete subjected to freeze-thaw process." *International Journal of Civil & Structural Engineering*, v. 5, n. 1, p. 42-52, 2014. ISSN 0976-4399.

Schreyer, H. "Continuum damage based on elastic projection operators." *International Journal of Damage Mechanics*, v. 4, n. 2, p. 171-195, 1995. ISSN 1056-7895.

Shang, H.; Song, Y. "Experimental study of strength and deformation of plain concrete under biaxial compression after freezing and thawing cycles." *Cement and Concrete Research*, v. 36, n. 10, p. 1857-1864, 2006. ISSN 0008-8846.

Shang, H.-S., Song, Y.-P. "Behavior of air-entrained concrete under the compression with constant confined stress after freeze–thaw cycles." *Cement and Concrete Composites*, v. 30, n. 9, p. 854-860, 2008. ISSN 0958-9465.

Shang, H.-S., Song, Y.-P., Qin, L.-K. "Experimental study on strength and deformation of plain concrete under triaxial compression after freeze-thaw cycles." *Building and Environment*, v. 43, n. 7, p. 1197-1204, 2008. ISSN 0360-1323.

Siemes, A. "Miner's rule with respect to plain concrete variable amplitude tests." *ACI Special Publication*, v. 75, 1982.

Smith, E. W., Pascoe, K. J. "Biaxial fatigue of a glass-fibre reinforced composite. Part 1: Fatigue and fracture behavior." Mechanical Engineering Publications: 367-396 p. 1989.

Smith, G., Young, L. "Ultimate theory in flexure by exponential function." ACI Journal Proceedings, 1955, ACI.

Song, Y., Ou, J. "Behavior of high water-cement ratio concrete under biaxial compression after freeze-thaw cycles." *Journal of Wuhan University of Technology-Mater. Sci. Ed.*, v. 23, n. 4, p. 589-594, 2008. ISSN 1000-2413.

Song, Y.-P., Cao, W., Meng, X.-H. "Fatigue properties of plain concrete under triaxial constant-amplitude tension-compression cyclic loading." *Journal of Shanghai University* (English Edition), v. 9, n. 2, p. 127-133, 2005. ISSN 1007-6417.

Su, E. C., Hsu, T. T. "Biaxial Compression Datigue and the Discontinuity of Concrete." *ACI Materials Journal*, v. 85, n. 3, 1988. ISSN 0889-325X.

Tepfers, R., Kutti, T. "Fatigue strength of plain, ordinary, and lightweight concrete." ACI Journal Proceedings, 1979, ACI.

Thapa, K., Yazdani, S. "A Strain Based Damage Model for structural Concrete." *Innovations in Structural Engineering and Construction*, 2008. p.753-756.

Torrenti, J.-M., Reynouard, J.-M., Pijaudier-Cabot, G. "Mechanical Behavior of Concrete." Wiley Online Library, 2010. ISBN 1848211783.

Truesdell, C., Baierlein, R. "Rational thermodynamics." *American Journal of Physics*, v. 53, n. 10, p. 1020-1021, 1985. ISSN 0002-9505.

Van Mier, J. G. M. "Strain-softening of concrete under multiaxial loading conditions." Technische Hogeschool Eindhoven, 1984.

Wastiels, J. "Behaviour of concrete under multiaxial stresses—a review." *Cement and Concrete Research*, v. 9, n. 1, p. 35-44, 1979. ISSN 0008-8846.

WEN, C. "Bounding surface approach to the fatigue modeling of engineering materials with applications to woven fabric composites and concrete." North Dakota State University, 2011. ISBN 1124652914.

WEN, C. et al. "Bounding Surface Approach to the Modeling of Anisotropic Fatigue Damage in Woven Fabric Composites." *Open Journal of Composite Materials*, v. 2, p. 125, 2012.

Yang, D. "A distribution function for the fatigue life of concrete." *Magazine of Concrete Research*, v. 46, n. 168, p. 215-222, 1994. ISSN 0024-9831.

Yazdani, S. "On a class of continuum damage mechanics theories." *International Journal of Damage Mechanics*, v. 2, n. 2, p. 162-176, 1993. ISSN 1056-7895.

Yazdani, S., Karnawat, S. "A constitutive theory for brittle solids with application to concrete." *International Journal of Damage Mechanics*, v. 5, n. 1, p. 93-110, 1996. ISSN 1056-7895.

Yin, W., Hsu, T. T. "Fatigue behavior of steel fiber reinforced concrete in uniaxial and biaxial compression." *ACI Materials Journa*l, v. 92, n. 1, 1995. ISSN 0889-325X.

Zhang, B., Phillips, D., Wu, K. "Effects of loading frequency and stress reversal on fatigue life of plain concrete." *Magazine of Concrete Research*, v. 48, n. 177, p. 361-375, 1996. ISSN 1751-763X.